

# Application of quality-controlled sea level height observation at the central East China Sea: Assessment of sea level rise

Taek-bum Jeong<sup>1,2</sup>, Yong Sun Kim<sup>3,4,57\*</sup>, Hyeonsoo Cha<sup>564</sup>, Kwang-Young Jeong<sup>675</sup>, ~~Mi-Jin~~  
~~Jang~~<sup>73</sup>, Jin-Yong Jeong<sup>886</sup>, and Jae-Ho Lee<sup>3\*</sup>

<sup>1</sup>Center for Climate Physics, Institute for Basic Science, Busan, Republic of Korea, 46241

<sup>2</sup>Pusan National University, Busan, Republic of Korea, 46241

<sup>3</sup>Ocean Circulation Research Center, Korea Institute of Ocean Science and Technology, Busan, Republic of Korea,  
49111

~~<sup>47</sup>Ocean Science, University of Science and Technology, Daejeon, Republic of Korea, 34113~~

<sup>5</sup>Ocean Science and Technology School, Korea Maritime and Ocean University, Busan, Republic of Korea, 49112

~~<sup>564</sup>~~Center for Sea-Level Changes, Jeju National University, Jeju, Republic of Korea, 63243

~~<sup>675</sup>~~Ocean Research Division, Korea Hydrographic and Oceanographic Agency, Busan, Republic of Korea, 49111

~~<sup>71</sup>YSK11National Disaster Management Research Institute, Ulsan, Republic of Korea, 44538~~

~~<sup>886</sup>~~Marine Disaster Research Center, Korea Institute of Ocean Science and Technology, Busan, Republic of Korea,  
49111

~~<sup>7</sup>Ocean Science, University of Science and Technology, Daejeon, Republic of Korea, 34113~~

26

27

28

29 *Correspondence to:* [Jae-Ho Lee \(Jaeholee@kiost.ac.kr\)](mailto:Jaeholee@kiost.ac.kr), [Yong Sun Kim \(yongskim@kiost.ac.kr\)](mailto:yongskim@kiost.ac.kr), ~~[Jae Ho Lee](mailto:Jaeholee@kiost.ac.kr)~~  
30 ~~[\(Jaeholee@kiost.ac.kr\)](mailto:Jaeholee@kiost.ac.kr)~~

31

---

## ~~Abstract~~

This study presents ~~the~~ a state-of-the-art quality control (QC) process for ~~the~~ sea level height (SLH) time series observed at the Jeodo Ocean Research Station (I-~~ROS~~ORS) in the central East China Sea, a unique in-situ measurement in the open sea for over two decades with a 10-minute interval. The newly developed QC procedure, ~~called~~ named the Temporally And Locally Optimized Detection (TALOD), ~~method~~ has two notable differences in characteristics from the typical ones: 1) spatiotemporally optimized local range check based on the high-resolution tidal prediction model TPXO9, 2) consideration of ~~the~~ the occurrence rate of a stuck value over a specific period. Besides, the TALOD adopts an extreme event flag (EEF) system to provide SLH characteristics during extreme weather. A comparison with the typical QC process, satellite altimetry, and reanalysis products demonstrated ~~s~~ that the TALOD method ~~could~~ can provide reliable SLH time series with few misclassifications. ~~A~~ Through budget analysis ~~suggested, it was determined~~ that the sea level rise at ~~the~~ I-ORS ~~was~~ primarily caused by the barystatic effect, and the trend differences between observations, satellite, and physical processes ~~were~~ are related to vertical land motion. It was confirmed ~~through Global Navigation Satellite System (GNSS)~~ GNSS that ground subsidence of  $-0.89 \pm 0.47$  mm/yr is occurring at I-ORS. As a representative of the East China Sea, this qualified SLH time series makes dynamics research possible spanning from a few hours of nonlinear waves to a decadal trend, along with simultaneously observed environmental variables from the air-sea monitoring system ~~at~~ in the research station. This TALOD QC method ~~was~~ is designed ~~to process~~ for SLH observations in the open ocean, but it can be generally applied to SLH data from tidal gauge stations in the coastal regions.

## 1 Introduction

Sea Level Height (SLH) comprises both oceanic components such as tides and currents, and atmospheric components (Pirooznia et al., 2016). Global warming, driven by due to the increased greenhouse gases, has caused led to a persistent increase in of heat fluxes into the ocean, accelerating the rise in the upper ocean heat content and the loss of land-based glaciers and ice sheets, resulting in rapid sea level rise (SLR; Pugh, 2019; Fox-KemperPirani, 2021IPCC[YSK2]). This rise is not spatially homogeneous but localized in association with a change in the current system (*e.g.*, Roemmich et al., 2007; Hamlington et al., 2020; Lee et al., 2022; Li et al., 2024). Rising sea levels have induced coastal erosion and broad flooding, suggesting a presumable vulnerability of populated low-lying coastal regions to global warming (Kulp and Strauss, 2019). Recent research has demonstrated its robust relationship with-between SLR and extreme weather events (Cayan et al., 2008; Yin et al., 2020; Calafat et al., 2022), underscoring the need for a long-term SLH monitoring network.

A global network of tidal gauges inat the coastal regions, along with satellite altimetry for the open ocean, has made it possible to observe worldwide sea level changes (*e.g.*, Dieng et al., 2017; Chen et al., 2017; Cazenave et al., 2018; Chen et al., 2017; Royston et al., 2020; Cha et al., 2023). The upward trend of global mean SLR increased from 3.05 mm/yr for the period 1993–2018 to 3.59 mm/yr from 2006 to 2018, about twice faster than 1.7 mm/yr during the 20<sup>th</sup> century (Nerem et al., 2018; Fox-Kemper et al., 2021; Nerem et al., 2018). TheA future projected future sea level trend is expected to be  $4.63 \pm 1.1$  mm/yr for the period 2010–2060, based on from observed and reconstructed measurements around Korea (Kim and Kim, 2017), implying more frequent occurrences of extreme weather and climate hazards associated with steep the mean sea level rising within the near future.

Due to theits broad socioeconomic implications of SLR, the Korea Hydrographic and Oceanographic Agency (KHOA) has constructed a sea level monitoring network comprising with thirty-eight38 tide gauge stations for the coastal region around Korea (red pentagram in Fig 1). Besides, the ocean research stations, steel-framed tower-type research facilities, started to conduct unceasing and autonomous observations to cover the north-south a north-south section of the Yellow and East China Seas, allowing us to understand air-sea interaction and atmospheric and oceanic processes onin various time scales overinat the open ocean (Kim et al., 2017; Ha et al., 2019; Kim et al., 2017; Kim et al., 2019; Kim et al., 2022; Kim et al., 2023a; Kim et al., 2023b; Saranya et al., 2024). The Jeodo ocean research stationOcean Research Station (I-ORS), the first one constructed at 32.125°N, 125.18°E (see Fig. 1 for its location), was established in 2003. It, has been producing sea level measurements using a radar-type sensor with a 10-minute interval for more than two decades since October 2003. This station is

strategically positioned along the pathway of typhoons that impact the Korean Peninsula; hence, the I-ORS can serve as a crucial platform for comprehending extreme weather phenomena (Moon et al., 2010; [Kim et al., 2017](#); [Park et al., 2019](#); [Yang et al., 2022](#)) and long-term climate variability ([Kim et al., 2023a](#)).

The collected sea level data, however, contains intricate outliers such as missing [data](#), spikes, electric noise, stucks, drift, systematic conversion (or offset)<sup>1</sup>, and so on (Pytharouli et al., 2018). These outliers must be identified or corrected before being used for research. This process, known as Quality Control (QC), involves outlier classification into range, variability (or gradient), and sensor test categories (OOI, 2013; Min et al., 2020). [Each institution utilizes a different algorithm.](#) ~~Numerous quality control (QC) methods have been proposed and developed to date. Recently, Lin Ye et al. (2023) reported that applying upgrades to the delayed-mode SEa LLevel NEar real time (SELENE) QC software improved the auto-flagging ability for tidal gauge sea level height (SLH) data by 1.6 %. Additionally, individual modules within QC systems are being specifically designed and evaluated to detect particular types of outliers.~~ [Each institution utilizes a different algorithm.](#) For instance, outliers might be identified by applying a threshold ~~that is 3-fold the~~ of three times the standard deviation above and below the average of measurements within a specified sliding window (Min et al., 2020; 2021). This approach assumes [the](#) Gaussian distribution of the observed time series; hence, it may not be suitable for ~~uniform application~~ uniformly applying this method because nonlinear waves or abrupt extreme events tend to be misclassified as outliers. ~~Also~~ [In addition](#), the variables that are greatly affected by strong tides may have difficulty detecting outliers when a range check is performed without considering tidal components. Therefore, Pugh (1987) suggested a QC procedure based on tidal components estimated by a harmonic analysis. ~~Recently~~, Pirooznia et al. (2019) computed tides by adopting the classical least squares (CLS) and total least squares (TLS) from raw data that contained outliers and missing values. They used the estimated tidal components to get residual components of SLH data and then performed outlier detection. ~~Numerous quality control (QC) methods have been proposed and developed to date.~~ [Recently, Lin-Ye et al. \(2023\) expanded the existing SEa LLevel NEar-real-time \(SELENE\) QC software by incorporating additional modules to enable delayed-mode QC. In particular, the harmonic analysis-based de-tiding module was upgraded to remove tidal components. The resulting time series has been effectively utilized to identify subtle anomalies such as spikes, attenuation, and datum shifts by eliminating the periodic tidal variability](#)

<sup>1</sup> The I-ORS methodology for sea level measurements was changed in December 2007. Previously, the I-ORS observed the length between the instrument and the sea level; since then, it has been changed to observe the sea level to the bottom. Due to the methodological switch, the recorded sea level time series has a sharp and systematic offset, as described in section 2.1.—

from the original observations. However, Recently, Lin Ye et al. (2023) reported that applying upgrades to the delayed-mode SEa-LEVEL NEar real-time (SELENE) QC software improved the auto-flagging ability for tidal gauge sea level height (SLH) data by 1.6 %. Additionally, individual modules within QC systems are being specifically designed and evaluated to detect particular types of outliers. This harmonic analysis-based process approach might be appropriate for the data stably obtained from tide gauge stations but seems impertinent to measurements in the open ocean, which may have various types of intricate outliers. The open ocean data not only exhibited more frequent and extreme errors but also showed fundamentally different error patterns that have not been observed in tide gauge measurements. Although the exact causes of these errors observed in the open ocean remain unclear, experienced researchers have consistently pointed to the unstable power supply as a likely contributing factor. [TJ3]

In addition, previous studies attempted to verify the factors contributing to sea level rise (SLR) using various data. Cha et al. (2023) quantified and assessed the underlying processes contributing to sea level rise in the Northwestern Pacific (NWP) using reanalysis data and satellite measurements from 1993 to 2017. This study they found that the major contributions to sea level rise SLR include are land ice melt and sterodynamic (STEROD) components, while the spatial pattern and interannual variability are dominated by the sterodynamic-STEROD effect. However, satellite-based sea level observations cannot detect vertical land motion such as subsidence or uplift, which may lead to trend differences between satellite and station observation. This indicates the need to analyze the variability of vertical land motion at these stations as well.

This paper aims to introduce a unique, invaluable SLH time series obtained in the open ocean over two decades, processed with a newly developed QC process named the Temporally And Locally Optimized Detection (TALOD) method. For this purpose, we take-took advantage of simulated tidal components based on the TOPEX/Poseidon global tidal model v9 (TPXO9; Erofeeva and Egbert, 2018). This high-resolution global tidal model accurately reproduces tidal-well components around the Korean Ppeninsula (Lee et al., 2022) and, hence, can be used for a local and temporal range check. The performance of the newly suggested QC process wasis assessed by comparing it to the a typical QC method suggested by the Intergovernmental Oceanographic Commission (IOC) KHOA method, which is based on the Intergovernmental Oceanographic Commission (IOC) Manual, and the qualified, daily and monthly averaged sea level time series are assessed using satellite altimetry and reanalyzed products from GLORYS12, ORAS5, and HYCOM regarding their long-term trends. Additionally, the physical processes contributing to sea level rise SLR at the I-ORS were analyzed using reanalyzed products, and the vertical land motion at the I-ORS platform was estimated using the Global Navigation Satellite System (GNSS).

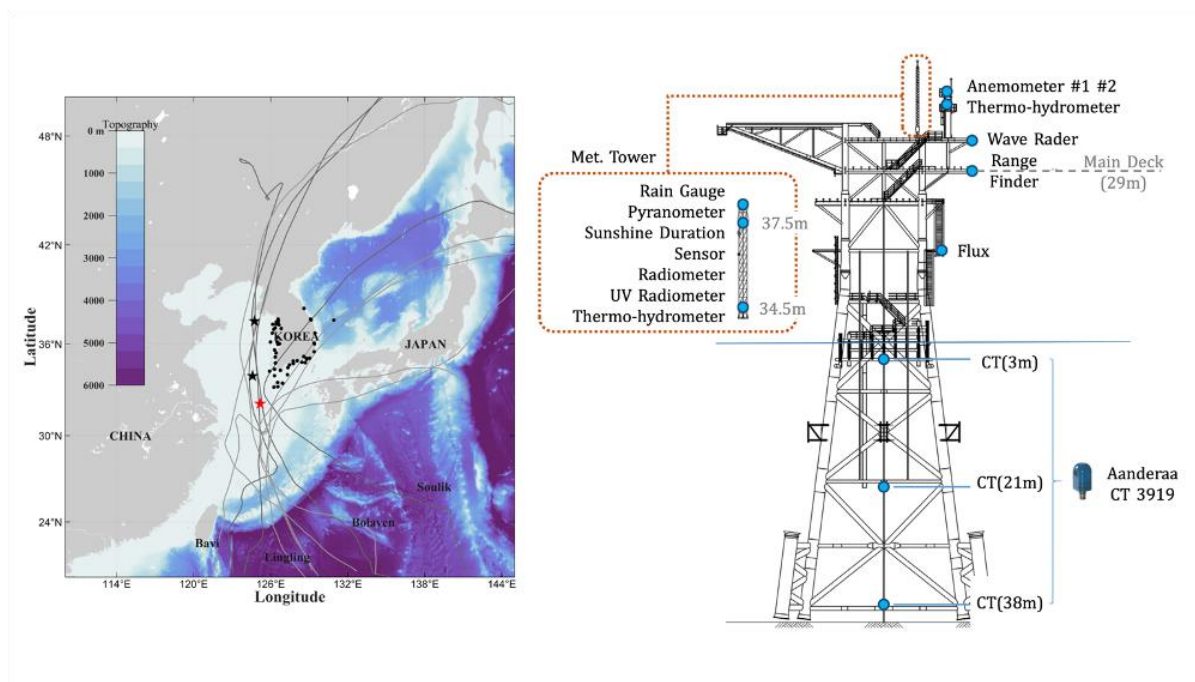
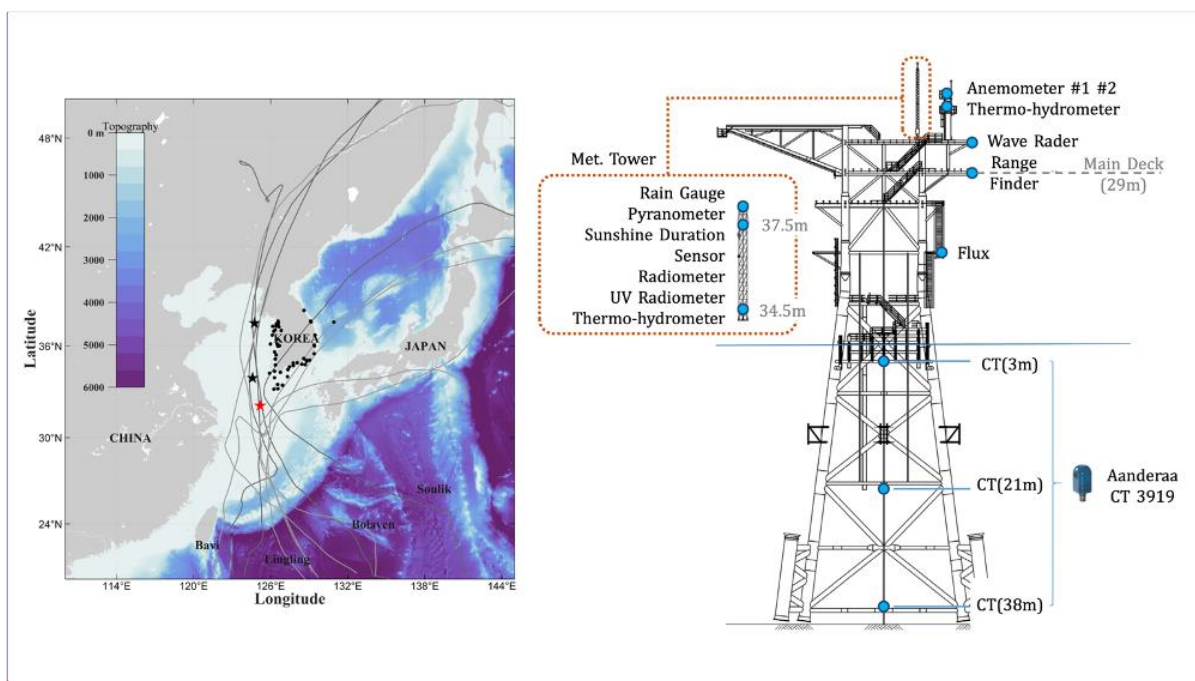


Figure 1. The structure of I-ORS and Instruments (Right) and the horizontal distribution for bathymetry and the tracks of typhoons passed by I-ORS (data from Joint Typhoon Warning Center; cases depicted in Fig. 6). The star marks indicate the location of the I-ORS (red) and the Socheongcho (black, north) and Gageocho (black, south) Ocean Research Stations. The black dots depict the locations of tide stations. The grey solid lines show the storm tracks passing by I-ORS from 2003 to 2022 (Table 2). The darker lines indicate the typhoon case in Fig. 6.



[TJ4]

**Figure 1.** The structure of I-ORS and Instruments (Right) and the horizontal distribution for bathymetry and the tracks of typhoons passed by I-ORS (data from Joint Typhoon Warning Center [YSK5]; cases depicted in Fig. 610). The star marks indicate the location of the I-ORS (red) and the Socheongcho (black; above) and Gageocho (black; below) Ocean Research Station, respectively. The black dots depict the locations of tide stations. The grey solid lines show the storm tracks passing by I-ORS from 2003 to 2022 (Table 2). The darker lines indicate the typhoon case in Table 2 Fig. 6.

## 2 Data and Methods

### 2.1 SLH observed time series from the I-ORS

We constructed the TALOD QC process based on the TPXO9 and applied it to the 10-minute interval real-time SLH measurements obtained from the I-ORS, a total of 1,011,584 data points from 8 October 2003 to 31 December 2022. The data were measured by using a MIROS SM-140 non-directional wave radar (MIROS AS, Asker, Norway), installed on the main deck 29 m above the sea surface (Fig. 1). The range-finder principally estimates the distance to the sea surface through using the reflected signals by detecting back-scattered microwaves from the surface. Table 1 describes the detailed specifications of the SM-140. The sensor's measurements are known to be relatively free from atmospheric conditions, such as rain, fog, and water spray.

As mentioned in the introduction, the sea level measuring standard was changed on 12 December 2007. A sharp offset of about approximately 6.7 m, therefore, was recorded between the data before and after the transition point (TP); (see Fig. 2). Before the TP, the range-finder recorded the distance from the sensor to the sea surface as sea level. After that, the KHOA then altered the standard to record the actual sea level by subtracting the measured distance from the known height off from the sea bottom floor to the sensor (KHOA, 2013). Therefore, in this study, the forepart was corrected the forepart by flipping-inverting it upside-down and then shifting-adjusting it by 1.57 m to the position extrapolated to the first time of the data afterwards. Also In addition, we performed the harmonic analysis within the corrected SLH time series to validate the correction method. The corrected SLH time series for December 2007 estimated a sufficiently high signal-to-noise ratio (SNR) over 10.0 (Pawlowicz et al., 2002), compared to the much broader ranges like years or decades of SLH at the I-ORS. Its consistencies in amplitude and phase consistency with the rear subset also guarantee the method for correcting the systematic offset.



Table 1. Instrument specifications for the MIROS SM-140.

<u>Data</u>	<u>Range</u>	<u>Resolution</u>	<u>Accuracy</u>
<u>Range</u>	<u>1 – 23 m</u>	<u>1 mm</u>	<u>&lt; 5 mm</u>
	<u>3 – 95 m</u>		
<u>Frequency</u>	<u>50 – 200 Hz (according to range)</u>		

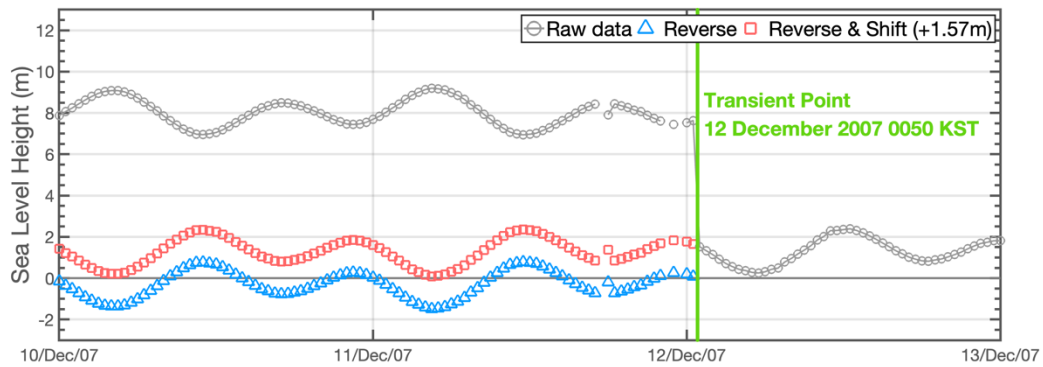
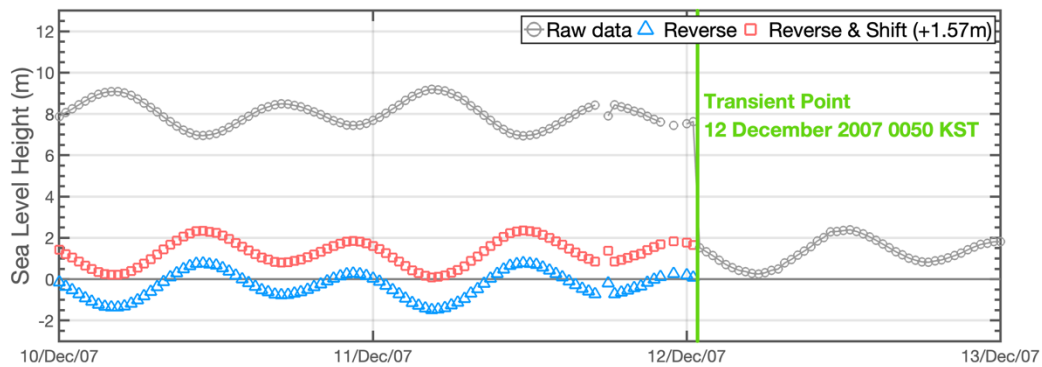


Figure 2. The circle markers indicate each process of methodological adjustment for the data before TP. The grey line with circles means the raw data and the lines with blue triangle and red square indicate the reverse and shift (+ 1.57 m after reversed) process.

Table 1. Instrument specifications for the MIROS SM-140 by MIROS.

<u>Data</u>	<u>Range</u>	<u>Resolution</u>	<u>Accuracy</u>
<u>Range</u>	<u>1 – 23 m</u>	<u>1 mm</u>	<u>&lt; 5 mm</u>
	<u>3 – 95 m</u>		
<u>Frequency</u>	<u>50 – 200 Hz (according to range)</u>		



**Figure 2. The circle markers indicate each process of methodological adjustment for the data before TP. The grey line with circles means the raw data and the lines with blue triangle and red square marker lines indicate the reverse and shift (+ 1.57m after reversed) process.**

### 2.1.1 Satellite altimetry and reanalysis products

We collected satellite altimetry and reanalysis datasets to validate the performance of the qualified SLH. The satellite ~~data were~~<sup>as is</sup> the gridded L4 sea surface height dataset provided by ~~the~~ Copernicus Marine Environment Monitoring Service (CMEMS, <https://doi.org/10.48670/moi-00145>) for 1993–2022. This altimetry, sea surface height from the geoid, was calculated through optimal interpolation (OI) by merging along-track altimetry from all satellites. Inverted barometric and tidal heights ~~corrections~~ <sup>were</sup> applied to adjust the along-track data. The daily gridded satellite altimetry has a quarter-degree resolution for the global ocean. We used ~~the~~ daily sea surface height (SSH) time series at the ~~nearest~~-grid point nearest to the I-ORS.

The three SSH products used in this study are the HYbrid Coordinate Ocean Model (HYCOM, <https://www.hycom.org/>) data-assimilative reanalysis (HYCOM-R) for the period of 2003-2017 and HYCOM non-assimilative simulation (HYCOM-S) from 2018 ~~to~~ -2022, Global Ocean Physics Reanalysis 12 version 1 (hereafter GLORYS; ~~Lellouche~~ Jean-Michel et al., 2021), and the Ocean Reanalysis System 5 (hereafter ORAS5; Zuo et al., 2019). The HYCOM product provided by the US Navy's operational Altimeter Processing System (ALPS) has a spatial resolution of  $1/12^\circ$  by  $1/12^\circ$  for the global ocean and a temporal resolution of 3 hours~~ly~~. GLORYS12 ~~was~~<sup>is</sup> produced by Mercator Ocean International (<https://www.mercator-ocean.fr/en/>) and has a spatial resolution of  $1/12^\circ$  by  $1/12^\circ$  for the global ocean with a daily resolution. The ORAS5<sub>2</sub> provided by the European Center~~e~~ for Medium-Range Weather Forecasts (ECMWF)<sub>2</sub> has a spatial resolution of  $1/4^\circ$  by  $1/4^\circ$  for the global ocean and a monthly temporal resolution ~~of monthly~~ (<https://doi.org/10.24381/cds.67e8eeb7>) (~~DOI: 10.24381/cds.67e8eeb7~~). To efficiently compare sea level variability, the SLH of all datasets ~~were~~<sup>as</sup> converted to sea level anomalies by subtracting their mean values. Except for ORAS5, which ~~contained~~<sup>is</sup> monthly data, the

other sea level data were averaged daily. Similarly, we estimated the daily mean observed time series when more than half of the data were available or flagged as good data.

## 2.1.2 Analysis on tide at the I-ORS

### 2.1.1 Satellite altimetry and reanalysis products

Harmonic analysis was conducted on the SLH observations during the well-observed period from March to June 2021. The M2 tide exhibits the largest amplitude of 0.62 m, with a signal-to-noise ratio (SNR) exceeding  $10^3$ . This tide is followed by S2 (0.32 m), K1 (0.20 m), N2 (0.16 m), and O1 (0.15 m). The mean amplitude of these primary constituents was 0.28 m, with an average SNR of approximately 3,000, notably higher than that of the remaining 31 constituents with amplitudes under 0.1 m (mean amplitude: 0.01 m, mean SNR: 6.01). [TJ6] [YSK7]

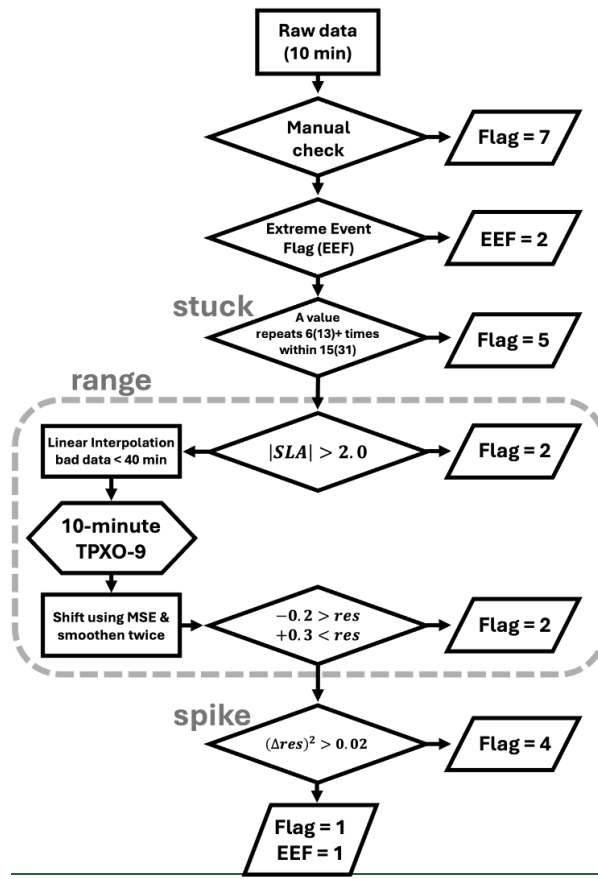
## 2.2 TALOD QC

### 2.2.1 ~~Meta-check~~ Manual Check

After correcting for the systematic offset in the observed sea level time series, we classified the outliers into four categories: ~~metadata manual~~, range, spike, and stuck (see Fig. 3 for a flowchart). Based on their understanding of the subsequent QC process, human operators ~~in the manual check~~ ~~subjectively~~ ~~electively~~ flag ~~only those data sections in the manual check sections~~—particularly those lasting more than 24 hours—that may ~~are likely to~~ disrupt automatic detection procedures. The metadata check involves manually flagging unreliable data, including ~~instrumental jolts or a data section that may disrupt the following automatic detection procedures to prevent~~ contamination of the observed data's long-term characteristics. This examination ~~should be~~ ~~is~~ ~~normally~~ based on historical metadata information (or field notes) on the sensor's maintenance, cleansing, ~~a~~ power shortage events ~~at in the ocean research of the~~ station, etc. Unfortunately, ~~metadata information concerning the observed SLH time series from the I-ORS~~ ~~the observed SLH time series from the I-ORS~~ ~~was~~ ~~are~~ not ~~made publicly available as distributed documentation with metadata information~~. Instead, ~~considering the following processes~~, we flagged ~~subjectively~~ ~~a~~ ~~sections~~ where the periodicity of the SLH data was irregular or nonsensical data existed for several days. For example, from June 2016 to July 2017, the sea level observations at the I-ORS involved two relocations and one replacement of the observational instrument, and the sea levels observed during this period were relatively low (not shown). As a result, 56,024 data points were flagged based on the ~~metadata manual~~ check accounting for 6.32% of the total observations. This study ~~points out~~ ~~emphasises~~ the ~~need~~ ~~significance~~ ~~offer~~ recorded metadata

238 information ~~into~~ ensuringe the quality assessment of ~~the~~ observed time series and facilitating efficient instrumental  
239 maintenance.

240



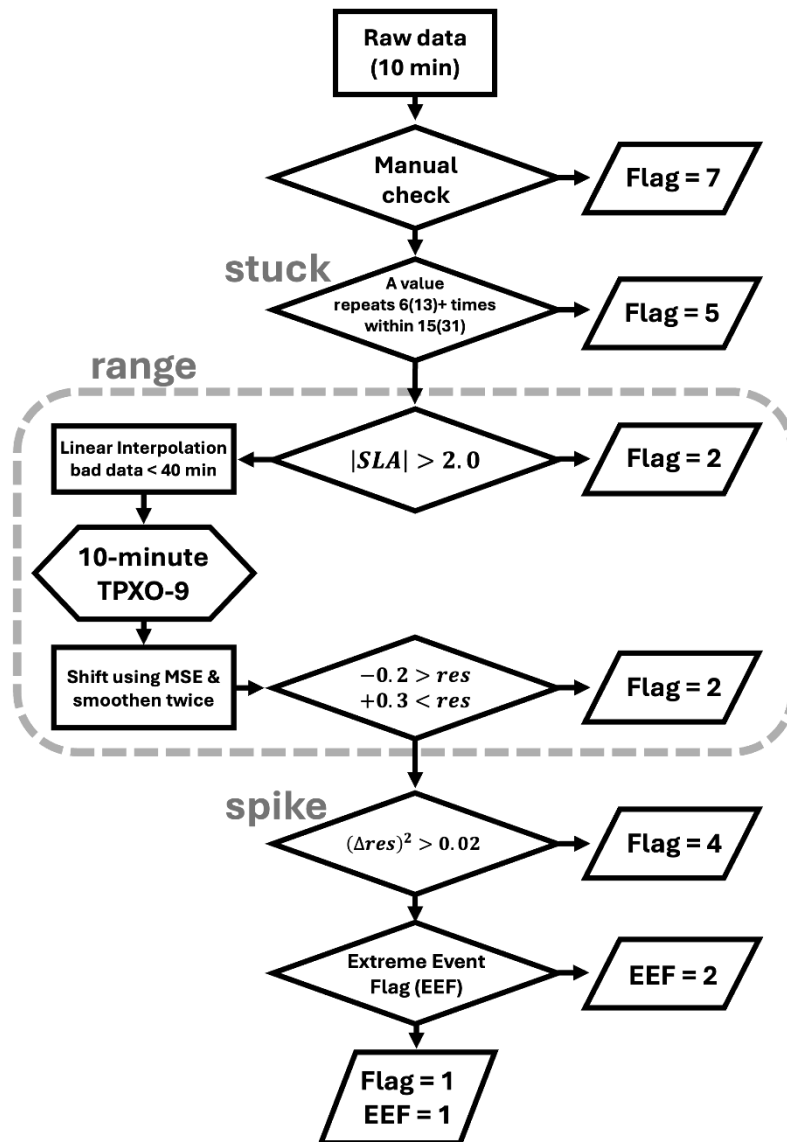


Figure 3. Flow chart of TALOD QC process.

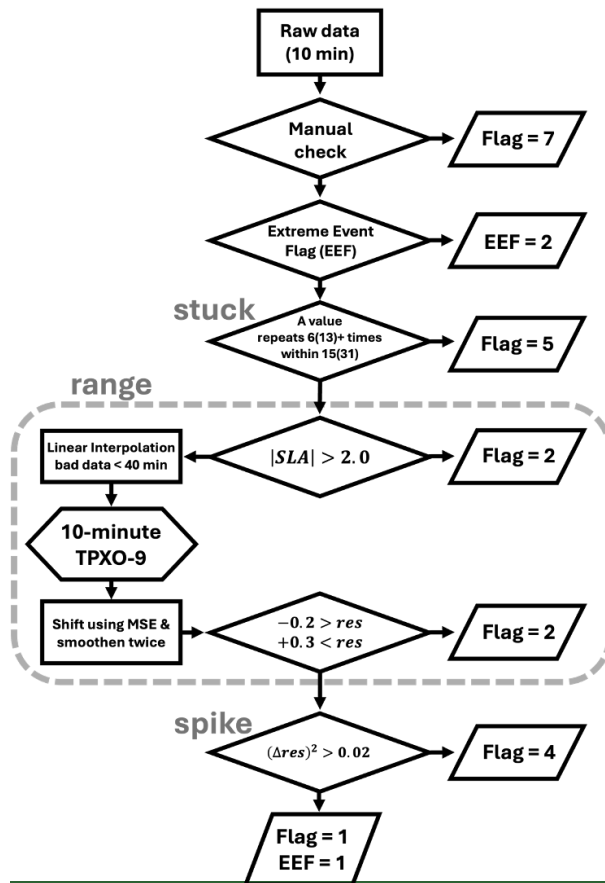


Figure 3. Flow chart of TALOD QC process.

### 2.2.2 Stuck check

After the metadata manual check, we recommend examining stuck values in the time series. Generally, a stuck check detects outliers when a fixed value is recorded continuously ~~recorded~~ over a certain period. At the I-ORS, the SLH measurements exhibited two distinct characteristics of stuck values. Firstly, these values persist for a certain duration without variation; a typical QC processes can identify this type kind of stuck. Second, a An abnormal case was observed at the I-ORS: alternation between normal observations (good data) and fixed values. To handle both this usual and unusual stuck cases efficiently, we adopted the density of identical values over a certain period through testing. ~~We experimented with various combinations of ranges and frequencies combinations;~~ consequently As a result, we flagged the cases in which when a single value was detected more than 6 times within a range of 15 or more than 13 times within a range of 31.

### 2.2.3 Range check

~~Normally~~Typically, the range check can be divided into two parts. A local or gross range check designates a single value that is difficult to occur naturally for a target variable at a specific location during the a monitoring span. And, seasonally varying range check effectively detects errors for variables dominated by seasonal variability, such as air or sea surface temperatures or humidity. However, these methods are not suitable for SLH measurements in shallow water with large tidal amplitudes, such as the maximum tidal amplitude of 2.5 m that can occur at the I-ORS, and significant seasonal cycles (Lee et al., 2006).

This study's range check consists of two procedures. The first is a gross range check with a fixed range, by assigning upper (+2.0 m) and lower (−2.0 m) limits for the sea level anomaly (SLA). The second is a localized check with temporally varying ranges by taking advantage of the tidal prediction model. The gross range check effectively identifies flags extremely abnormally high values such as 29.0 m and 7.98 m, which are frequently recorded in the SLH measurements from the I-ORS, even during under normal weather situations conditions. For the local range check, we used the TPXO9 tidal model, which has a  $1/30^\circ$  horizontal resolution of  $1/30^\circ$ . This global tide model seems to offers provide accurate realistic tidal predictions in both space and time spatial and temporal tides around the Korean Peninsula, exhibiting with the smallest root mean square difference (RMSD) when compared to with tide gauge observations (Lee et al., 2022).

The monthly tidal data, consisting composed of 15 constituents (M2, S2, N2, K2, 2N2, K1, O1, P1, Q1, Mf, Mm, M4, MN4, MS4, and S1), were extracted from the TPXO9 and, sliding every month was were as adjusted using the observed SLH during for the same period (Fig. 4). Harmonic analysis of the observed SLH at the I-ORS shows that the M2 tide has the largest amplitude of 0.62 m. The M2 tide at the I-ORS, harmonic analysis result from the observed SLH, exhibits the largest amplitude of 0.62 m. This tide is followed by S2 (0.32 m), K1 (0.20 m), N2 (0.16 m), and O1 (0.15 m). The mean amplitude of these primary constituents was is 0.28 m, which is notably higher than that of the remaining 31 constituents with amplitudes under under 0.1 m. A monthly windows is were is selected to consider the seasonal evolution. The extracted tidal time series were as shifted to positions where that minimised the rRoot mMean sSquare eErrors (RMSEs), as indicated by were are minimized (the red line in Fig. 4). Overshooting tends to be generated occur when only using the arithmetic mean only for is used for the shifting, especially in for the convex-up and convex-down patterns data, which correspond to high and low tides, respectively. This may lead to the, thus potentially resulting in detecting the detection of overestimated outliers. To address mitigate this overshooting issue, the residual time series, i.e., the observations minus mean-shifted tides, was is smoothed twice and then added back to the estimated tidal



time series, as shown in ~~the~~ (the green line in Fig. 4). When the difference between the observed SLH and the bias-corrected tide exceeds +0.3 meters or falls below -0.2 meters, the local range check identifies the data points~~it~~ as ~~an~~-outliers (see Fig. 5b). These thresholds are ~~sufficient~~-adequate for elevation changes associated with nonlinear internal waves in this region (Lee et al., 2006).

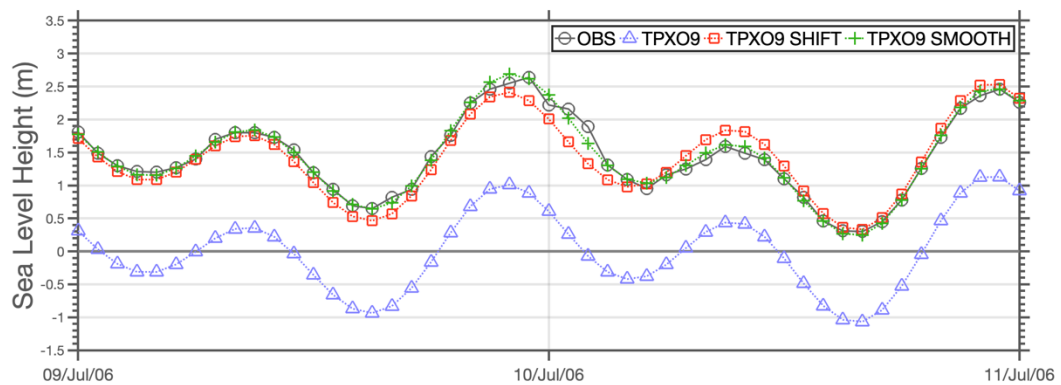


Figure 4. Lines indicate the processes for fitting TPXO9 to the observation (black line with circle) in the range check. (1) The blue line with a triangle means raw TPXO9 data. (2) The orange line with the square shows mean-shifted TPXO9 based on the mean square error method. (3) The green line with a circle indicates the final output with a twice-smoothed bias added.

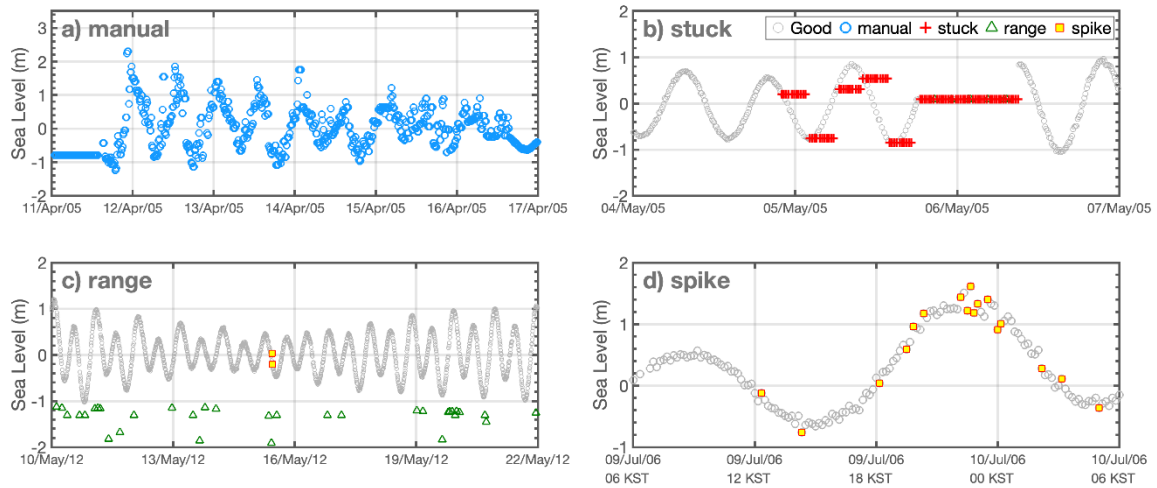
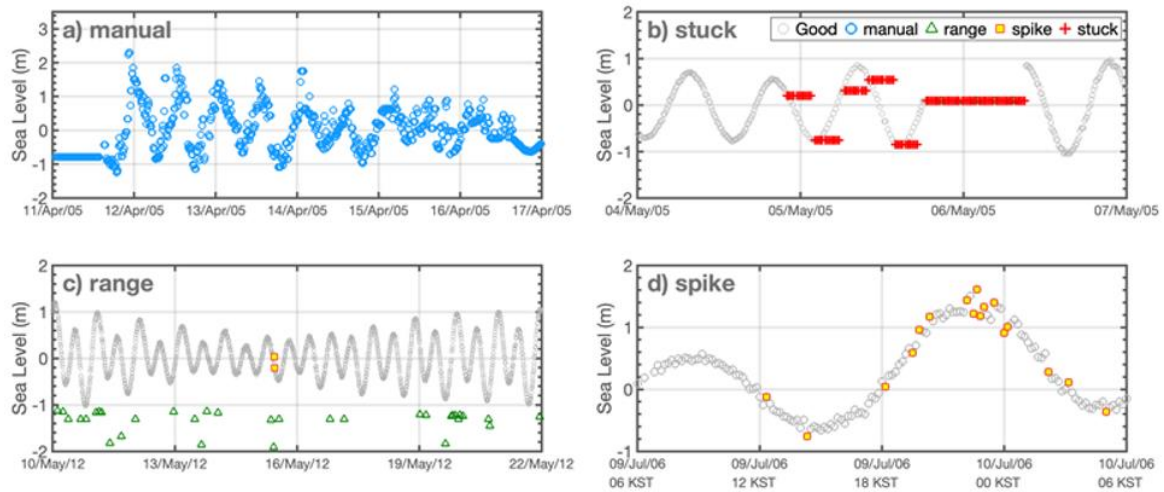


Figure 5. Time series for the examples of 4 flags. a) manual, b) stuck, c) range, and d) spike. Each marker indicates Good data (grey circle), manual (blue circle), range (green triangle), spike (yellow square with red outline), and stuck (red cross), respectively. Time series of the non-tidal residual component corresponding to Fig. 5 is provided in the Supplement (Fig. S1).

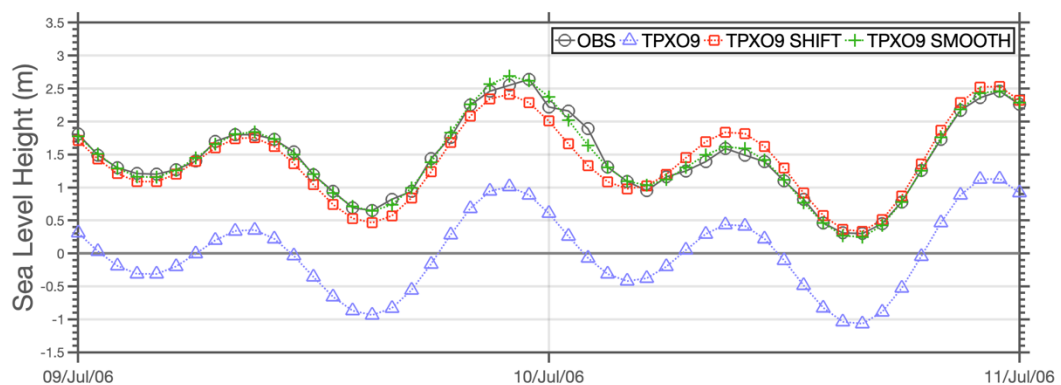
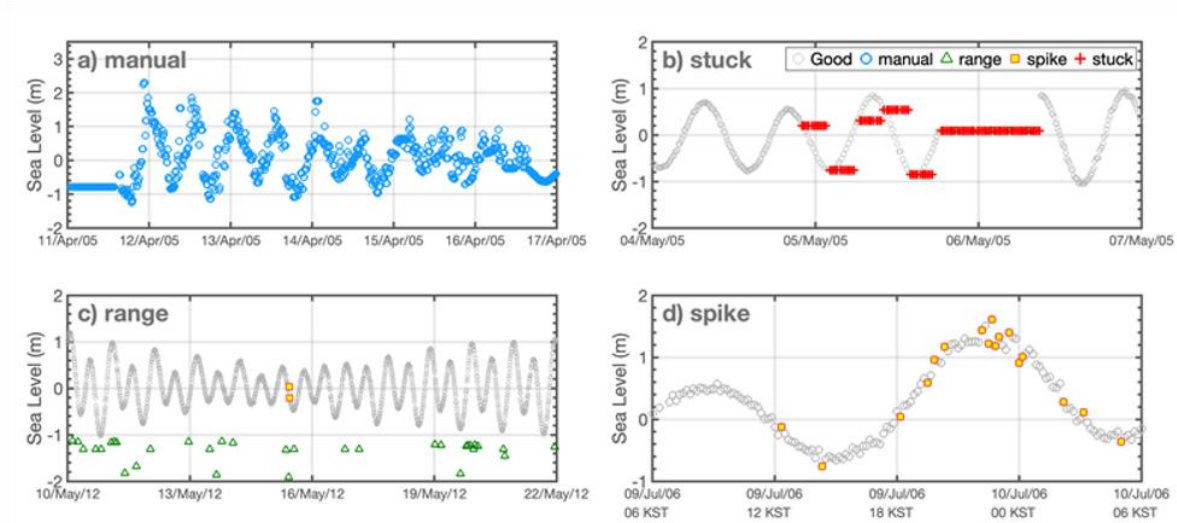


Figure 4. Lines indicate the processes for fitting TPX09 to observation (black line with circle) in the range check. (1) The blue line with a triangle means raw TPX09 data. (2) The orange line with the square shows mean-shifted

TPXO9 based on the Mean Square Error method. (3) The green line with a circle indicates the final output with a twice-smoothed bias added.



**Figure 5. Time series for the examples of 4 flags. a) metadata manual, b) rangestuck, c) spikerange, and d) stuckspike. Each marker indicates Good Data (grey circle), metadata manual (blue circle), range (green triangle), spike (yellow square with red outline), and stuck (red cross), respectively.**

## 2.2.4 Spike check

The spike check was developed based on the gGradient sSpike mMethod (GSM), following the approach of Hwang et al. (2022). The GSM generally typically detects identifies outliers using by evaluating the gradient of the SLH data. However, in this study, we employed utilised the temporal discrepancies in the non-tidal residual SLH time series. Specifically, a data point is classified as a spike, i.e. that is, if the square of its that value gradient exceeds 0.02, it is classified as a spike. The equation used is as follows:

$$flag = find((\Delta residual)^2 > 0.02), \quad (1)$$

## 2.2.5 Extreme event flag

Atmospheric factors such as sea level pressure and wind modulate SLH; the inverted barometer effect (IBE) and strong winds can generate abrupt SLH fluctuations in SHL. Under extreme weather conditions, the SLH measurements may be classified as an outliers through range and spike checks. However, the flagged SLH data flagged during severe weather events might may be regarded as good data reliable, depending on the situation. As a final last QC procedure, this study introduced the extreme event flag (EEF) to provide allow users with an

option to ~~with an option to utilize~~ the data based on their scientific objectives, ~~to note that the SLH data was~~  
~~measured over severe weather periods.~~ The typhoon cases analyzed in this study are ~~summarised~~~~shown~~ in Table  
 2.

The observed range of ~~SSH sea surface height~~ anomalies was ~~almost equal~~~~nearly identical under~~ ~~for~~ both normal  
 and typhoon situations, i.e., 0.30/–0.20 m and 0.29/–0.20 m, respectively. However, ~~the variance differed~~  
~~markedly, there was a significant difference in variance, which imp~~~~indicating~~~~ies large substantial~~ fluctuations in  
 the SLH measurements. The ~~variance during normal case exhibited a variance of~~~~conditions was~~ 9.0 cm<sup>2</sup>, whereas  
~~during the typhoon-influenced period,~~ it increased to 40 cm<sup>2</sup> ~~during the typhoon-affected period,~~ approximately a  
~~five5-fold~~~~five times~~ ~~rise~~~~higher.~~ ~~Consequently~~~~As a result,~~ although the maximum ~~and~~ /minimum ranges of ~~the~~  
 residual components remained almost unchanged during typhoon ~~periods,~~ the outliers classified by the spikes  
 increased significantly (Fig. 6). We manually flagged the typhoon periods with the EEf based on the daily  
 variance and ~~typhoon reports issued by the reported information on typhoons from the~~ ~~Korea Meteorological~~  
~~Administration (KMA).~~

Table 2. List of Typhoon during observation.

<u>Typhoon</u>	<u>Start date</u>	<u>End date</u>
<u>Chanthu (2021)</u>	<u>14 Sep, 2021</u>	<u>16 Sep, 2021</u>
<u>Bavi (2020)</u>	<u>25 Aug, 2020</u>	<u>26 Aug, 2020</u>
<u>Lingling (2019)</u>	<u>6 Sep, 2019</u>	<u>7 Sep, 2019</u>
<u>Kong-rey (2018)</u>	<u>6 Sep, 2018</u>	<u>7 Sep, 2018</u>
<u>Soulik (2018)</u>	<u>22 Aug, 2018</u>	<u>23 Aug, 2018</u>
<u>Chan-hom (2015)</u>	<u>12 Jul, 2015</u>	<u>12 Jul, 2015</u>
<u>Neoguri (2014)</u>	<u>9 Aug, 2014</u>	<u>9 Aug, 2014</u>
<u>Bolaven (2012)</u>	<u>27 Aug, 2012</u>	<u>28 Aug, 2012</u>
<u>Muifa (2011)</u>	<u>8 Aug, 2011</u>	<u>9 Aug, 2011</u>
<u>Megi (2004)</u>	<u>10 Aug, 2004</u>	<u>10 Aug, 2004</u>

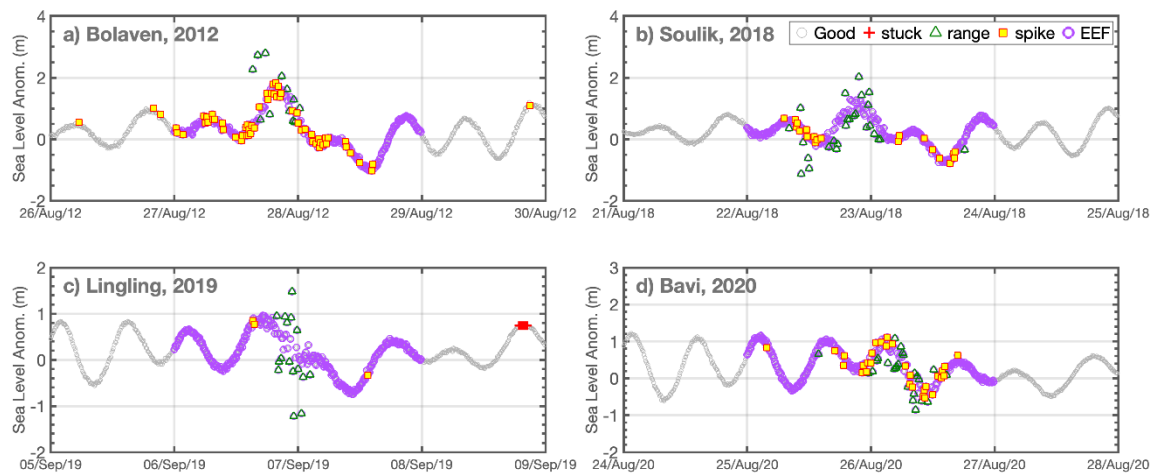
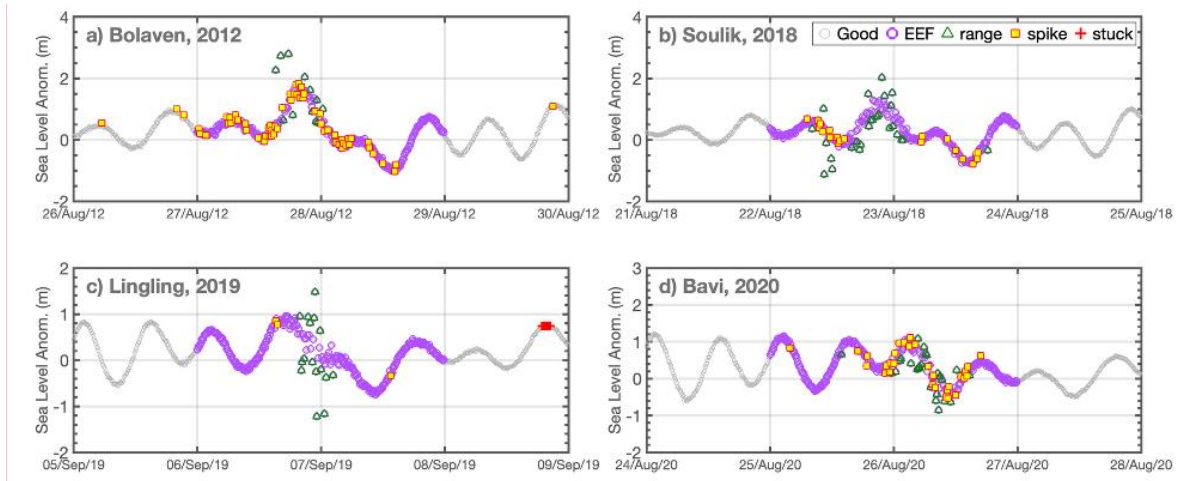


Figure 6. Time series of sea level anomalies for typhoon cases. a) Bolaven in 2012, b) Soulik in 2018, c) Lingling in 2019, and d) Bavi in 2020. Good data (grey circle), EEF (purple circle), range (green triangle), and spike (yellow square with red outline), respectively. Time series of the non-tidal residual component corresponding to Fig. 6 is provided in the Supplement (Fig. S2).

**Table 2.** List of Typhoon cases during observation.

Typhoon	Start-date	End-date
<b>Chanthu (2021)</b>	14 Sep, 2021	16 Sep, 2021
<b>Bavi (2020)</b>	25 Aug, 2020	26 Aug, 2020
<b>Lingling (2019)</b>	6 Sep, 2019	7 Sep, 2019
<b>Kong-rey (2018)</b>	6 Sep, 2018	7 Sep, 2018
<b>Soulik (2018)</b>	22 Aug, 2018	23 Aug, 2018
<b>Chan-hom (2015)</b>	12 Jul, 2015	12 Jul, 2015
<b>Neoguri (2014)</b>	9 Aug, 2014	9 Aug, 2014
<b>Bolaven (2012)</b>	27 Aug, 2012	28 Aug, 2012
<b>Muifa (2011)</b>	8 Aug, 2011	9 Aug, 2011
<b>Megi (2004)</b>	10 Aug, 2004	10 Aug, 2004



**Figure 6.** Time series of sea level anomalies for typhoon cases. a) Bolaven in 2012, b) Soulik in 2018, c) Lingling in 2019, and d) Bavi in 2020. Good Data (grey circle), EEF (purple circle), range (green triangle), and spike (yellow square with red outline), respectively. Same as Fig. 5, but for Typhoon cases.

### 3 Results

#### 3.1 Comparative analysis to existing QC process

Representative results obtained from during the TALOD QC process are shown in Figure 7, and the number and proportion of outliers and proportions flagged by each QC procedure are presented in Table 3. The results were compared with those obtained by applying the IOC's standard KHOA QC procedure, which follows based on the IOC manuals (IOC, 1990; IOC, 1993) and the NOAA handbook (NOAA, 2009), to assess the performance of the TALOD QC process. The IOC KHOA QC process comprised several steps was designed and implemented applied as a QC procedure consisting of several steps to accordance with international standards through the support from the National Data Buoy Center (NDBC) and the National Science Foundation under the National Oceanic and Atmospheric Administration (NOAA) to provide uniformly qualified observations to scientists (Min et al., 2020). The differences between these two QC processes are illustrated in Figure 8 and summarized in Table 4.

We collected a total of 1,011,584 SLH data points were collected from observed at the I-ORS during the observation period from 2003 to 2022. After excluding 165,702 instances of with missing values (NaNs), 886,128 data points were kept remained for quality control and analysis. Of these, 793,034 (89.49%) were classified as good data, while 93,184 data points (10.51%) were flagged as bad through the TALOD QC procedure (Table 3). Among the flagged data, excluding those flagged through the manual check, stuck values

constituted the majority, representing 89.84% of the bad data. This was followed by the spike and range flags, which accounted ed for 5.52% and 4.64% of the bad data, respectively.

Seasonal patterns in the frequency of each flag were further analyzed. The number of ~~occurrences of~~ bad data occurrences was ~~found to be the~~ highest in spring, exceeding the annual average by a factor of 1.28. This seasonal increase was primarily driven by the higher ~~occurrence-incidence~~ rate of stuck errors. Specifically, a total of 33,383 stuck errors were recorded, of which with 16,536 ~~instances occurred~~ in spring, the highest ~~count~~ across among all seasons (winter: 5,795; summer: 7,985; autumn: 3,067). The spring frequency of stuck errors in spring was nearly approximately double twice the annual average ~~(1.98 times)~~, presumably reflecting the influence of surface-drifting plankton on the rangefinder's reflection rate during the spring bloom period.

Other types of bad data ~~types~~, such as those flagged for range and spike errors, exhibited relatively low frequencies throughout ~~the whole seasons~~, with total counts of 1,725 and 2,052, respectively. In contrast, Conversely, the manual meta -flagged data, which accounted-represented for the largest proportion of bad data, ~~excluding NaN values, were evenly displayed a uniform-distribution across throughout the year all seasons~~, with a mean of 56,024 occurrences (winter: 14,934; spring: 12,298; summer: 14,843; autumn: 13,949). As a result Consequently, from a long-term perspective, the manual meta flag did not contribute significantly to the observed seasonal variation. ~~s in the from a long term perspective.~~

~~The~~ Overshooting-like errors flagged under the range and spikes categories ~~related to extreme weather conditions, such as range and spike flags showed~~ showed peak occurrence rates during in summer. This seasonal pattern coincided with the ~~peak~~ typhoon season ~~over over~~ the Northwestern Pacific WP, indicating a link age between extreme weather events and the occurrence of ~~overshooting-like~~ such error ~~s~~ types. Nevertheless, we recognize that the data for this period may be regarded as valid depending on the specific research objectives. Accordingly, an EEF has been implemented to enable researchers to include it in their analysis as good data. [TJ9]

The SLH is dominated by neap-spring tidal cycles, ~~which and it~~ can ~~induce-lead to~~ misclassifications in error detection when using through by a range check ~~that adopts a with a~~ constant ~~value as a~~ threshold. However In contrast, the TALOD method utilizes-employs residual components that ~~consider-account for~~ the rapid increase and decrease in of SLH caused by ~~most~~ diurnal tidal components and short-duration weather systems, thereby reducing detection errors. For example, the range check in the TALOD QC process successfully flagged 1,936 data points as by outliers. ~~In detail~~ Specifically, the gross range check ~~detected-identified~~ 1,121 bad data, while whereas the temporal and local outlier detection flagged an additional 815, efficiently capturing error-like values. identified 815 instances of bad data. As a result Consequently, the temporally and locally utilized outlier detection



~~method successfully captured the errors with little biases.~~ [YSK10] The TALOD QC process preemptively flags ~~anomalous~~ ~~bad values~~ ~~data~~ that ~~excessively~~ ~~severely~~ disrupt continuity through the range checks. This approach, as ~~depicted~~ ~~illustrated~~ in ~~Figure~~ ~~Fig.~~ 8f, prevents ~~sed~~ detection failures caused by recurrent spike-like errors ~~values~~. In contrast, ~~t~~ ~~The IOC's KHOA's~~ spike check has trouble with flagging spike-type errors ~~within that occur~~ ~~within~~ a short ~~time span~~ ~~period~~. These unqualified outliers ~~ying values may can~~ ~~provoke the downgrading~~ ~~cause a~~ ~~downgrade in~~ the performance of the spike ~~algorithms that rely on check using min/max-based for calculating to~~ ~~calculate~~ threshold ~~calculations~~. Attention should be ~~given paid~~ when applying the ~~IOC KHOA~~ QC processes to such sea level measurements, ~~as its~~ ~~because the~~ automatic QC ~~on observation data~~ ~~may could~~ be vulnerable to ~~recurrently~~ ~~repeatedly~~ recorded spike-like errors. For instance, among the 261 observations logged from 1 June 2016 00 KST to 14 June 2016 00 KST, the TALOD method flagged 43 instances as bad data, ~~w~~ ~~here~~ ~~as~~ ~~hile~~ ~~the~~ ~~IOC KHOA method~~ identified ~~only~~ 37, ~~leaving values only with~~ apparent error-like ~~values data still~~ ~~remaining unflagged~~ (see Fig. 8e, ~~and~~ 8f).

Moreover, as summariz~~ed~~ in Table 4, the two QC processes showed ~~significant~~ ~~remarkable~~ differences in ~~handling~~ the stuck checks. ~~While~~ ~~Although~~ ~~While~~ the TALOD QC process successfully detected~~s~~ stuck values, as illustrated in Fig. ~~ure~~ 8a, ~~8c,~~ ~~8e,~~ ~~and~~ ~~8g,~~ the ~~IOC KHOA method failed~~ ~~seems to fail~~ to identify these error-like values. Instead of flagging ~~the~~ abnormal stuck values, the ~~KHOA IOC~~ QC remove~~eds~~ the entire ~~data section~~ ~~segments~~ (Fig. 8b, ~~8d,~~ ~~8f,~~ ~~and~~ ~~8h~~). Furthermore, the ~~IOC's KHOA's~~ stuck check, which is designed to identify values as stuck when the sensor records the same values, tends to ~~misclassify~~ ~~excessively~~ normal ~~observations data~~ ~~into as~~ stuck errors due to instrumental ~~issues~~ ~~limitations~~ including low frequency (10-minute ~~intervals~~); ~~these~~ ~~Such misclassifications~~ ~~situations~~ are frequently observed during high and ~~neap~~ tides (Fig. 8d). ~~Fig. S3~~ ~~in the Supplement presents additional comparative results using the SELENE method proposed by Lin-Ye et al. (2023). SELENE failed to detect stuck errors in which NaN values alternated repeatedly with specific fixed values (Fig. S3c). Moreover, in the range and spike checks, it tended to misclassify or fail to detect errors when two or more overshooting values occurred consecutively (Fig. S3i).~~

During the application of the ~~IOC PKHOA~~ process to SLH data, misclassifications or detection failures were confirmed due to the inability to identify irregularly ~~recurring~~ ~~repeated~~ stuck errors. ~~However~~ ~~In contrast~~, the TALOD ~~method~~ applie~~d~~ optimiz~~ed~~ detection techniques; and ~~successfully flagged~~ 45,850 ~~stuck errors were~~ ~~successfully flagged~~. Fig. ~~ure~~ 9 shows the distribution of ~~the~~ observed and qualified SLAs. Compared ~~to~~ ~~with~~ the idealiz~~ed~~ normal distribution (indicated by the grey line in Fig. ~~ure~~ 9), unusually high ~~values~~ ~~frequencies~~ were concentrated in the ranges of -1.4 to -1.3 m, -0.2 to -0.1 m, and 0.4 to 0.5 m. After ~~applying~~ the TALOD QC,



this distribution ~~was aligned~~ is more closely ~~aligned~~ with the normal distribution, indirectly suggesting the performance effectiveness of the TALOD QC to identify outliers. The KHOA QC, meanwhile, appears to flag an excessive amount of data as outliers, resulting in a distribution that deviates significantly from normality (see dark grey distribution in Fig. 9).

Table 3. Detection counts and proportions for each flag from Oct 2003 to Dec 2022 (excluding NaN values).

<u>Flag number</u>	<u>1</u>	<u>2</u>	<u>4</u>	<u>5</u>	<u>7</u>	<u>8</u>
<u>(Name)</u>	<u>(Good data)</u>	<u>(Range)</u>	<u>(Spike)</u>	<u>(Stuck)</u>	<u>(Manual)</u>	<u>(NaN)</u>
<u>#</u>	<u>793,034</u>	<u>1,725</u>	<u>2,052</u>	<u>33,383</u>	<u>56,024</u>	<u>165,702</u>
<u>% (without NaN)</u>	<u>89.49%</u>	<u>0.19%</u>	<u>0.23%</u>	<u>3.77%</u>	<u>6.32%</u>	

Table 4: Differences in flag detection methods between TALOD and KHOA.

<u>Flag</u>	<u>TALOD</u>	<u>KHOA</u>
<u>Range</u>	Data point where observation exceeds the threshold from the tidal component, which is adjusted according to temporal observations	Data point exceeds sensor or operator-selected min/max for whole period
<u>SPIKE</u>	Data point where the square of the difference in residuals exceeds the threshold	Data point n-1 exceeds a selected threshold relative to adjacent data points
<u>STUCK</u>	Data point where the reoccurrence rates for constant value within the windows are over thresholds	Invariant value

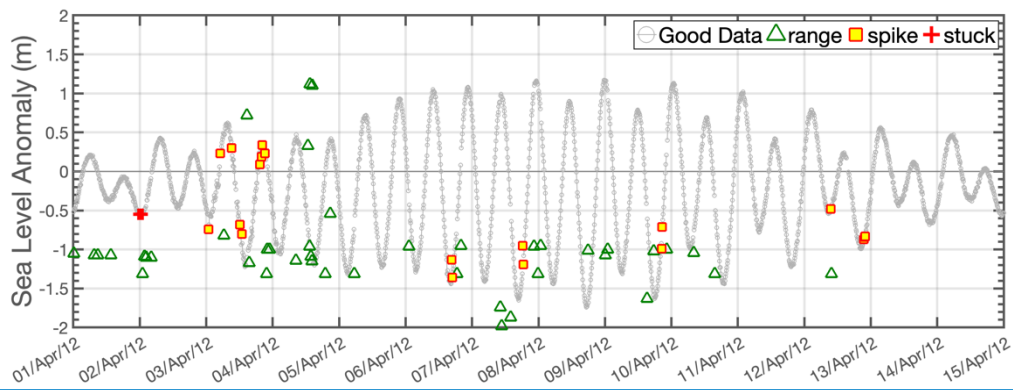


Figure 7. Representative results from 01 Apr 2012 to 15 Apr 2012.

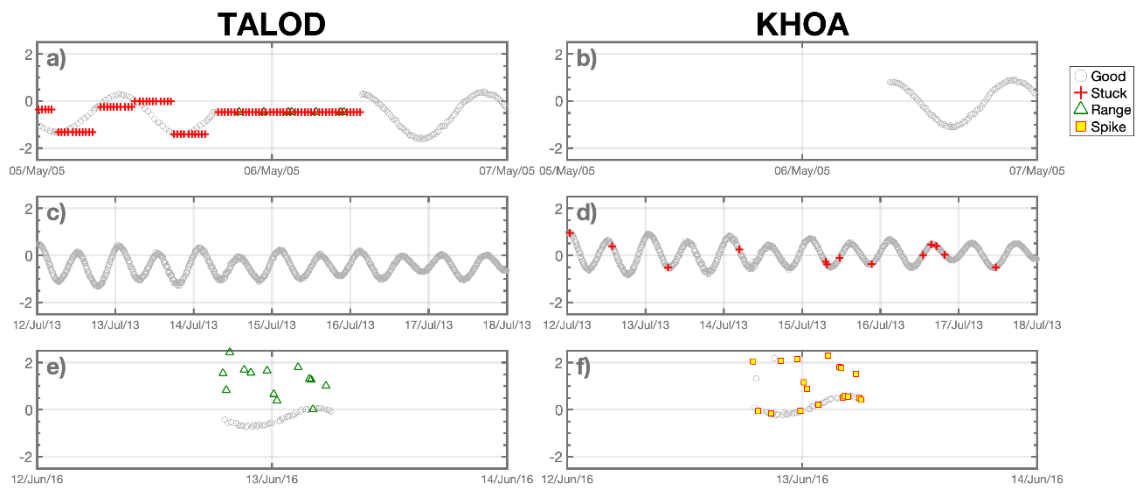


Figure 8. Same as Fig. 5, but for invariant stuck case (a-b, from 05 May 2005 to 07 May 2005), stuck case during short-period (c-d, from 12 Jul 2013 to 18 Jul 2013), and range-spike misclassification case (e-f, from 12 Jun 2016 to 14 Jun 2016). The figures on the left and right sides show results for TALOD and KHOA, respectively. For illustrative purposes, only the flags generated by the automatic QC process were considered in panel f. Comparison results with SELENE are provided in the Supplement (Fig. S3).

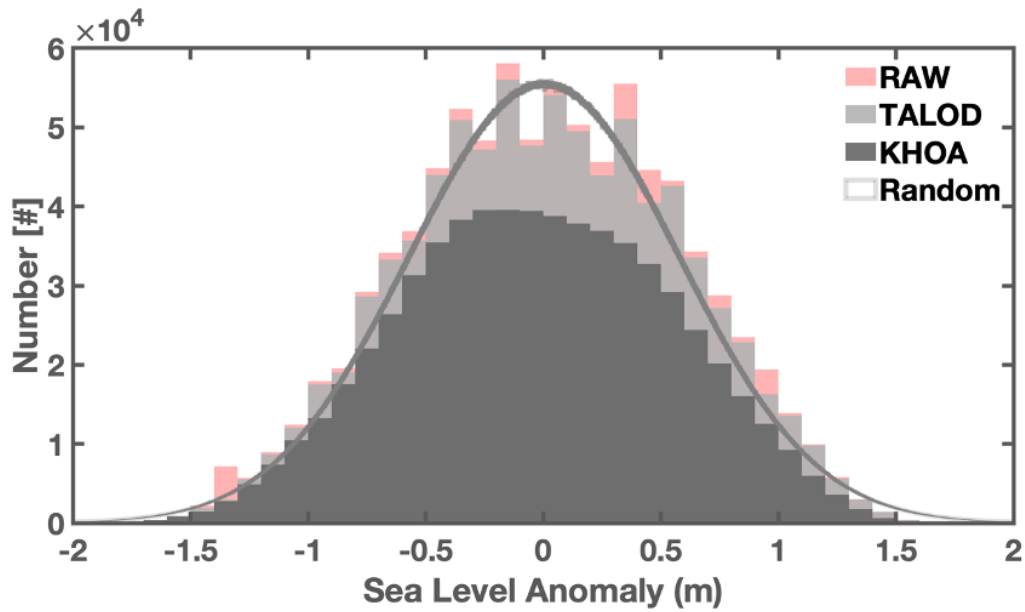


Figure 9. Histogram of observed sea level anomalies without QC (light red), with QC (light grey), QCed by KHOA method (dark grey) from 2003 to 2022 at the I-ORS. The area enclosed by a darker grey line indicates the normal distribution.

**Table 3.** Detection counts and proportions for each flag from Oct 2003 to Dec 2022 (excluding NaN values).

Flag-number (Name)	1 (Good data)	2 (Range)	4 (Spike)	5 (Stuck)	7 (MetadataM annual)	8 (NaN)
#	793,034	1,725	2,052	33,383	56,024	165,702
% (without NaN)	89.49%	0.19%	0.23%	3.77%	6.32%	

**Table 4:** The differences in flag detection methods between TALOD and KHOA.

Flag	TALOD	KHOA
Range	Data point where observation exceeds the threshold from the tidal component, which is adjusted according to temporal observations	Data point exceeds sensor or operator selected min/max for whole period

<b>SPIKE</b>	Data point where the square of the difference in residuals exceeds the threshold	Data point n-1 exceeds a selected threshold relative to adjacent data points
<b>STUCK</b>	Data point where the recurrence rates for constant value within the windows are over thresholds	Invariant value

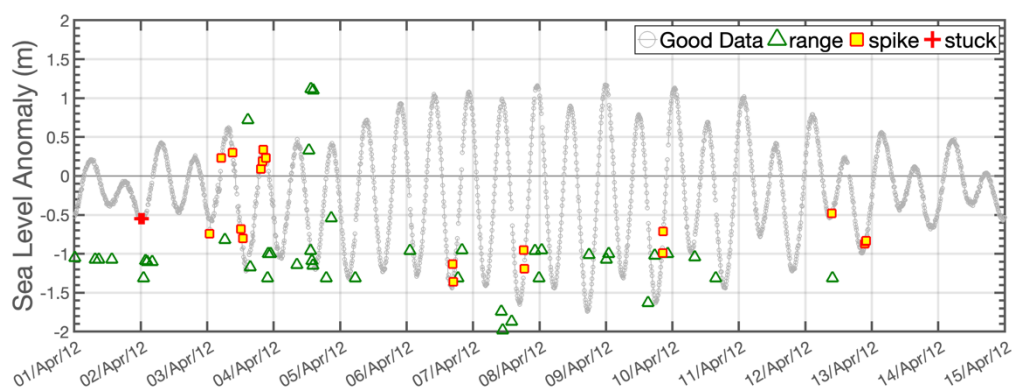
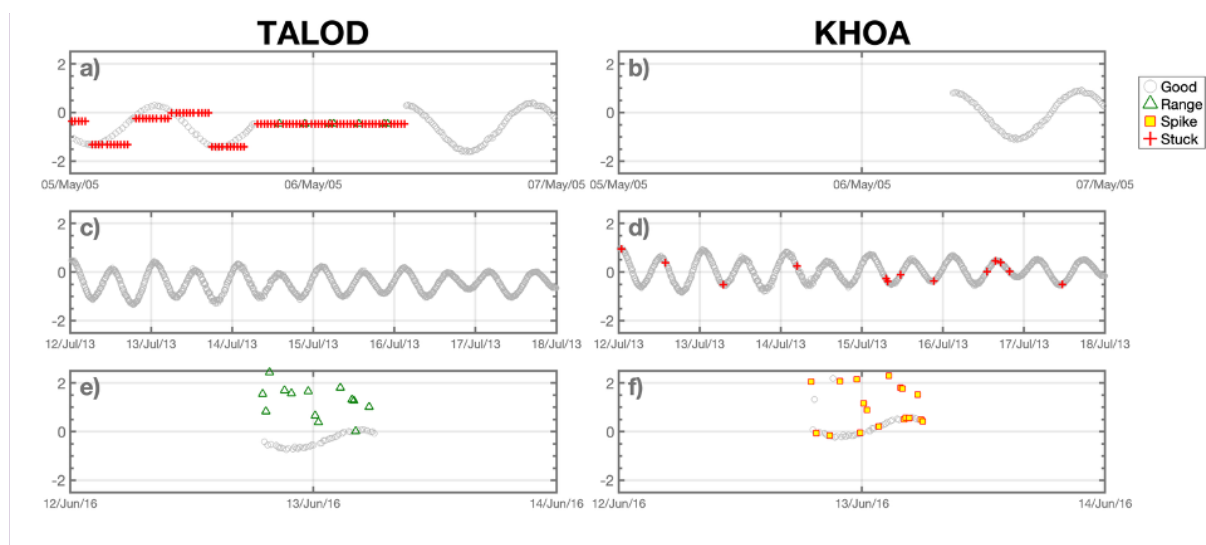


**Figure 7. Representative results from 01 Apr 2012 to 15 Apr 2012.**



[TJ11]

**Figure 8.** Same as Fig. 5, but for invariant stuck case (a-b, from 05 May 2005 to 07 May 2005), stuck case during short period (c-d, from 12 Jul 2013 to 18 Jul 2013), and range spike misclassification case (e-f, from 12 Jun 2016 to 14 Jun 2016), and range spike mixed case (g-h, 08 Sep 2016 to 13 Sep 2016). The figures on the left and right sides show results for TALOD and IOCKHOA, respectively. For illustrative purposes, only the flags generated by the automatic QC process were considered in panel f.

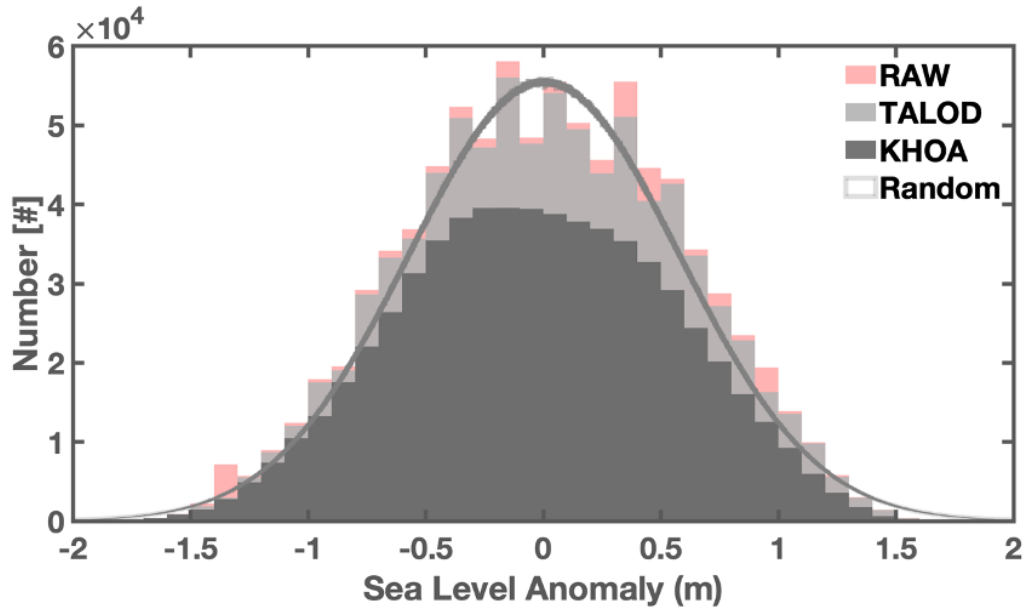


**Figure 9.** Histogram of observed sea level anomalies without QC (light red), and with QC (light grey), QCed by KHOA method (dark grey) from 2003 to 2022 at the I-ORS. The area enclosed by a darker grey line indicates the normal distribution.

### 3.2 Data validation by using observation data

Figure 10 displays the daily time series of the SLA for each dataset except ORAS5. SLH generally represents the vertically integrated heat contents of the ocean. Therefore, there are higher (lower) SLAs were observed during the boreal summer (winter) period, June-September (December-March), and lower SLAs during the boreal winter, December-March. The daily mean sea level range was approximately  $\pm 0.6$  m for the observed data,  $-0.4$  to  $+0.6$  m for the HYCOM product, and  $\pm 0.3$  m for GLORYS and satellite altimetry. We calculated the standard deviation (STD) and variance of each dataset, to infer their variability and distribution. The STD and variance for the I-ORS measurements were 0.16 m and 0.02 m, respectively. For satellite altimetry and GLORYS, the values were the same identical at 0.10 m and 0.01 m, for the HYCOM-R, had values of 0.11 m and 0.01 m, respectively. While, Both satellite altimetry and the two reanalysis datasets simulated exhibited lower SLH variability of SLH compared to that of the in-situ observations. However, both datasets they captured the overall pattern well, showing high accuracy with a low RMSEs (of less than 0.1 m). Compared to HYCOM, which has a spatial resolution of  $1/12^\circ$  and a temporal resolution of 3 hourly, the satellite altimetry data exhibits lower seasonal variance, which might be due to the substantial optimal interpolation procedure to reduce high frequency noise during a gridding process. Notably, distinct significant statistical differences were found observed between in the HYCOM and dataset other datasets (OBS and reanalysis data) for the period after 2018. Therefore, Accordingly, we divided further analyzed the HYCOM dataset by dividing it into two periods for further analysis: before 2018 (HYCOM-R) and after 2018 (HYCOM-S).

First, we compared ~~the~~ SLR ~~rates-trend~~ of each dataset (Fig. 11a). The observation exhibited an SLR of 5.27 mm/yr ~~for this over the~~ period ~~from~~ 2003 ~~to~~ 2022, while the satellite altimetry ~~data showed a rendered slightly~~ lower rates of 2.76 mm/yr. ~~Owing-Due~~ to a ~~robuststrong and unrealistic falling-declining~~ trend in the HYCOM's SLA during the recent period ~~since 2018~~ (-24.42 mm/yr ~~since 2018 for~~; HYCOM-S), the overall ~~rate-of~~ SLR ~~rate~~ for the HYCOM was negative (-4.22 mm/yr) ~~overduring~~ the full study period. ~~butIn contrast, the~~ HYCOM-R ~~has-aexhibited a more reasonable trend of~~ 2.70 mm/yr ~~trend~~ from 2003 to 2017. ~~These results might~~ ~~indicateshighlight the need for caution that we must be careful~~ when using the HYCOM-R and HYCOM-S products to ~~investigatestudy~~ long-term climate dynamics.

Figure 11a shows the monthly sea level trends for the observation and ~~the~~ other four datasets. The observation ~~showed a higher sea level rise~~ SLR rate ( $5.27 \pm 0.46$  mm/yr) compared to the other datasets. ORAS5 exhibited a ~~trend similar to satellite altimetry, while GLORYS and HYCOM showed a falling sea level fall trend. As mentioned earlier, HYCOM showed a strong fall decreasing trend unlike other datasets because it simulated lower sea levels after 2018.~~

~~Second~~Also, we ~~compared-assessed~~ the correlation and variability between the observation ~~data~~ and the other four datasets using a Taylor ~~d~~Diagram (Fig. 11b). ~~Among the datasets, s~~ Satellite altimetry ~~exhibited-showed~~ the highest accuracy ~~among the datasets~~, with a ~~high-strong~~ correlation coefficient ~~of~~ (0.71) and a low RMSE (0.04 m) ~~compared-relative withto~~ the observation. ~~The For~~ HYCOM, ~~it~~ reanalysis showed the lowest correlation coefficient ( $-0.08$ ) and ~~the~~ highest RMSE (0.10 m) over the entire period, indicating poor agreement. ~~While~~ HYCOM-R demonstrated performance ~~close-to~~comparable to ~~that-of-s~~ Satellite altimetry, ~~whereas~~ HYCOM-S ~~exhibited-showed~~ a significantly low correlation coefficient ( $-0.39$ ) and a high RMSE (0.12 m). ~~ORAS5 and GLORYS had~~ The correlation coefficients ~~of ORAS5 and GLORYS were~~of 0.71 and 0.76, respectively, ~~and thewith both~~ RMSEs of ~~both data was~~ 0.1 m, ~~showing-demonstrating higher-better correlation-agreement~~ and accuracy than ~~those-of~~ HYCOM. Overall, HYCOM ~~performed poorly, primarily because of~~ was found to have an ~~overall lower performance due to~~ its inability to ~~simulate-reproduce SLH the~~ variability ~~inof SLH sinceafter~~ 2018 in ~~the~~ HYCOM-S product.

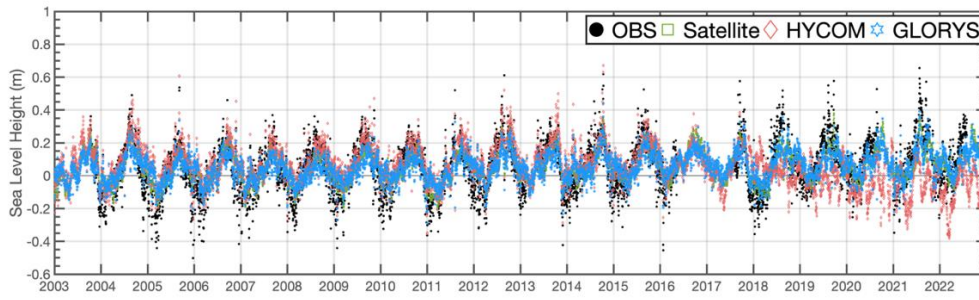


Figure 10. Time series of daily mean sea level data after observations (black dot), satellite altimetry (green empty circle), HYCOM (light red diamond), and GLORYS12 (light cyan hexagram) data during the observation period at the I-ORS.

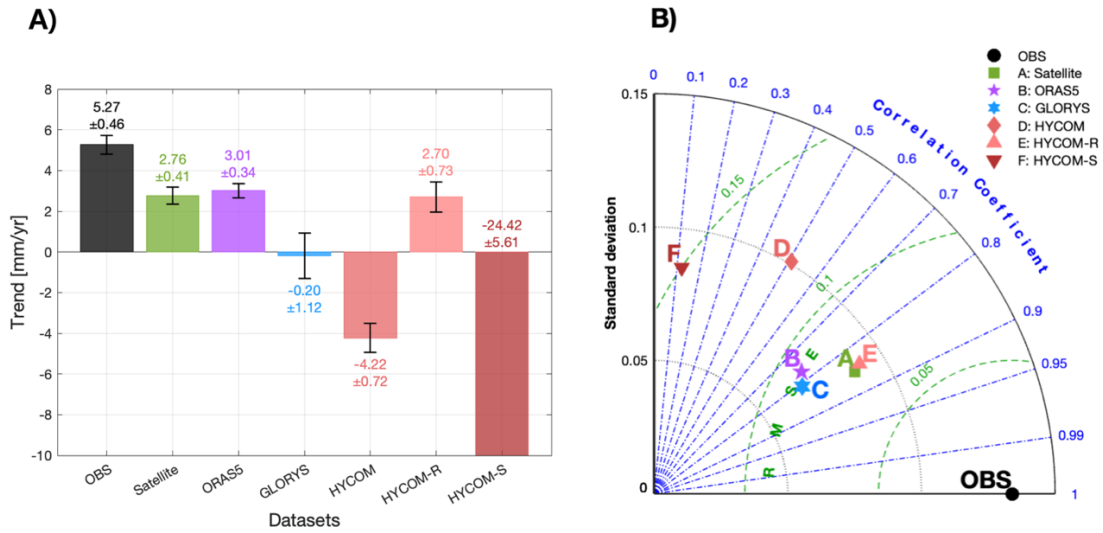
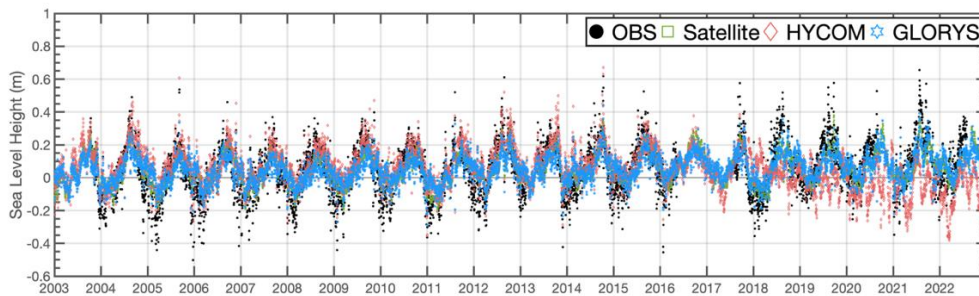
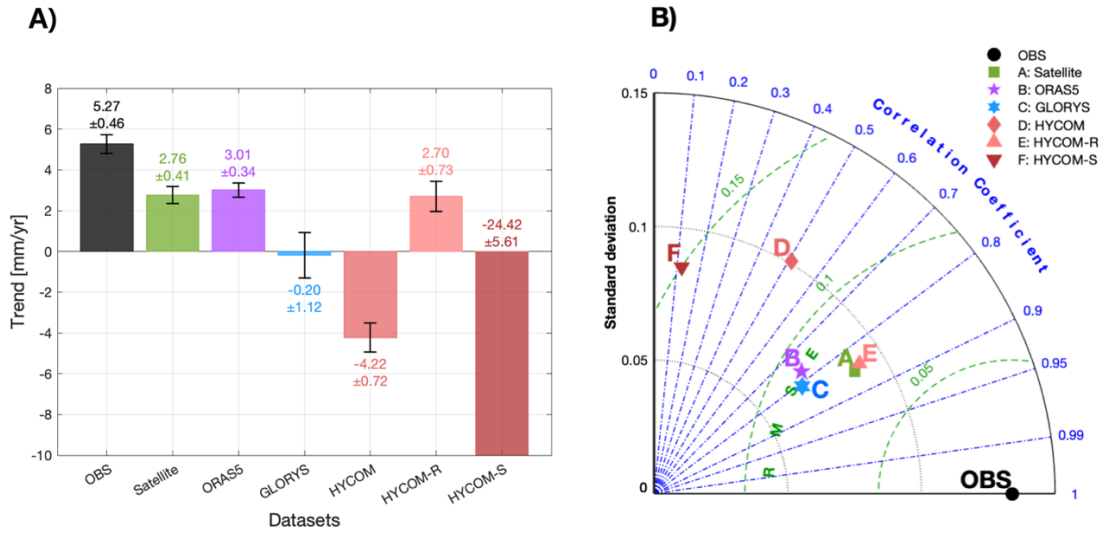


Figure 11. Bar plot with error bar (A; Left) and modified Taylor diagram (B; Right). The azimuthal angle represents the correlation coefficient, the radial distance indicates the standard deviation, and the semicircles centered at the “OBS” marker mean the Root Mean Square Errors. The colors and markers indicate each dataset (black circle: observation, green square: satellite altimetry, purple pentagram: ORAS5, light cyan hexagram: GLORYS, red diamond: HYCOM, light red upward-pointing triangle: HYCOM-R, dark red downward-pointing triangle: HYCOM-S).





**Figure 10. Time series of monthly daily QC-ed observations (black dot), Satellite (green empty circle), HYCOM (light red diamond), and GLORYS12 (light cyan hexagram) data during the observation period at the I-ORS.**



**Figure 11. Bar plot with error bar (A; Left) and Modified Taylor diagram (B; Right). The azimuthal angle represents the correlation coefficient, the radial distance indicates the standard deviation, and the semicircles centered at the “OBS” marker mean the Root Mean Square Errors. The colors and markers indicate each dataset (black circle: observation, green square: Satellite altimetry, purple pentagram: ORAS5, light cyan hexagram: GLORYS, purple pentagram: ORAS5, red diamond: HYCOM, light red upward-pointing triangle: HYCOM-R, light dark red downward-pointing triangle: HYCOM-S).**

### 3.3 Sea-level budget assessment at I-ORS

As mentioned above, the SLH observations from the I-ORS, produced refined through the developed QC process, estimated an SLR rate of  $5.27 \pm 0.46$  mm/yr. Sea level changes are categorized into relative and geocentric sea level change, referring to the height of the sea surface relative to representing the distance from the sea floor and the Earth's center of the earth to the sea surface, respectively. The ground-based observations, such as those from the I-ORS, represent the relative sea level change, and this change variation is influenced by various physical processes, including sea-level changes due to ocean density and circulation, i.e., the ~~(sterodynamic SD)~~sterodynamic (SDTERO) effect, mass exchange between the ocean and land, i.e., the ~~(barystatic BSARY)~~barystatic (BSARY) effect, and glacial isostatic adjustment (GIA) (Gregory et al., 2019; Frederikse et al., 2020; Cha et al., 2024). In this regard, we performed a budget analysis of each physical process that affecting the SLR at the I-ORS.

The ~~sterodynamic (STEROD)~~sterodynamic effect is calculated as the sum of the dynamic sea level change (DSL) and the global mean steric sea level rise SLR (GMSSL) (Gregory et al., 2019). DSL was obtained from using ORAS5, which was also used for validation data in this study. GMSSL used in situ observation data was derived from in situ observational datasets provided by the Institute of Atmospheric Physics (IAP; Cheng et al., 2017), the Met Office Hadley Centre (EN4; Good et al., 2013), and the Japan Meteorological Agency (JMA; Ishii et al., 2017).



The GMSSL was produced using the temperature-salinity profile data from each institution and was used to compute the  $\Delta T_{\text{ERO}}$  effect by adding the DSL. The  $\Delta B_{\text{ARYS}}$  effect refers to sea level rise resulting from mass contributions of ice is the sum of ice-melting from the Antarctica, and Greenland ice sheets, glaciers, and changes in land water storage. For this, we used the reconstructed ocean mass reconstructed  $\Delta B_{\text{ARYS}}$  data from Ludwigsen et al. (2024). The GIA comprises accounts for sea level changes due to the disappearance-redistribution of mass due to the melting and retreat of glaciers since the last glacial period, and. To estimate GIA, we used the model outputs from Caron et al. (2018), who Caron et al. (2018) improved model accuracy by incorporating utilized a global positioning system (GPS) time series from 459 sites and 11,451 relative sea level records, as well as by data to improve the model accuracy, and based on this, computing the ensemble mean of 128,000 model simulations.

Figure 12 presents the sea level time series and trend budget at the I-ORS along with a comparison with satellite altimetry data. The rate of sea level change rate SLR due to contributed to physical processes ( $\text{Sum} = \Delta T_{\text{ERO}} + \Delta B_{\text{ARYS}} + \text{GIA}$ ) was  $2.57 \pm 0.35$  mm/yr, which is about approximately  $2.70 \pm 0.58$  smaller than the that of observation ( $5.27 \pm 0.46$  mm/yr). A similar discrepancy was also found when comparing satellite altimetry to observation (difference:  $2.51 \pm 0.62$  mm/yr). Among the components of physical processes, the  $\Delta T_{\text{ERO}}$  effect contributed  $0.73 \pm 0.34$  mm/yr, accounting for approximately 28% of the total estimated SLR rise. The  $\Delta B_{\text{ARYS}}$  effect contributed the most had the largest contribution, with a  $1.85 \pm 0.02$  mm/yr (about approximately 72%). Meanwhile, GIA led to resulted in a slight fall in sea level falls, contributing  $-0.11 \pm 0.00$  mm/yr, about approximately 0.04%.

Satellites cannot are unable to detect vertical land motion (VLM) because they measure the changes in the distance from the center of the Earth to the sea surface. In contrast, whereas station-based observations such as I-ORS are affected by VLM, as because they measure the change in height from the sea-floor to sea level (Han et al., 2014; Gregory et al., 2019; Cha et al., 2024). Thus Hence, the difference between the sea level trend from satellite altimetry and that record at the I-ORS can be regarded as the VLM component. We checked examined whether the observed difference of approximately  $2.51 \pm 0.62$  mm/yr was could be associated with attributed to VLM. Cha et al. (2024) defined the total VLM as the sum of the VLM components in from GIA,  $\Delta B_{\text{ARYS}}$  effects, and local processes, where GIA and  $\Delta B_{\text{ARYS}}$  are categorized as represent natural processes contributions. The VLM of GIA-related VLM was obtained from Caron et al. (2018), while the VLM of  $\Delta B_{\text{ARYS}}$ -related VLM was derived from used the data of Frederikse et al. (2020), and. The VLM component of the local process was calculated using as the difference between the sea level change trend due to physical processes ( $2.57 \pm 0.35$  mm/yr) and the

observed sea level change trend of from observation ( $5.27 \pm 0.46$  mm/yr). At the I-ORS location, the VLM contributions from GIA and BARYS effects were calculated to be  $0.22 \pm 0.14$  mm/yr and  $0.28 \pm 0.64$  mm/yr, respectively. In contrast, the VLM one for BS-local processes was  $0.28 \pm 0.64$  mm/yr, and the VLM of the local process was  $-2.67 \pm 0.60$  mm/yr. Therefore, the total VLM was estimated at approximately  $-2.47 \pm 0.89$  mm/yr. Therefore, the total VLM was approximately  $-2.17 \pm 0.89$  mm/yr, indicating that significant ground subsidence is occurring at the site, principally driven by local factors rather than natural processes. at the I-ORS location, and this subsidence was more affected by local processes than by natural effects such as GIA and BS.

Additionally, we analyzed the trend of the observed vertical displacements using the Global Navigation Satellite System (GNSS data collected) at observing 30-second intervals at the I-ORS from 2013 to 2019. The trend of GNSS-derived vertical displacements, based on daily means, was  $-0.89 \pm 0.47$  mm/yr ( $p < 0.05$ ), using daily mean. Although this trend is estimated over a relatively short period and it's smaller lower than the estimated VLM from the local process ( $-2.67 \pm 0.60$  mm/yr), but it appears to certify confirmed the presence of that the actual ground subsidence exists at the I-ORS.



Figure 12. Monthly time series of sea level anomalies (left) and sea level rise rates (right; units: mm/yr). Each color and type of line indicates the dataset (OBS: black solid line, Satellite: green dotted line, Sum: bright red circle, STERO: orange diamond, BARY: purple dotted line, GIA: sea green dashed line, and GNSS: dark brown).

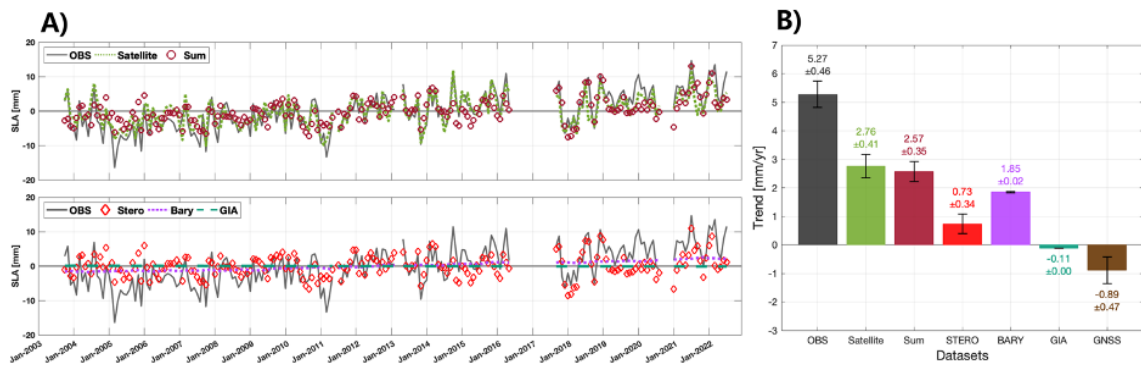


**Figure 12. Monthly time series of sea level anomalies (left) and bar chart with error bar for sea level rise rates (right; units: mm/yr). Each color and type of line indicates the dataset (OBS: black solid line, Satellite: green solid dotted line, Sum: bright red solid line with circle, STERO: orange diamond, BARY: purple dotted line, GIA: sky-blue dotted line, and GNSS: bright dark brown).**

#### 4 Summary and Discussion

This study developed a novel ~~quality control~~QC procedure named TALOD, based on a high-resolution tidal prediction model, ~~named the Temporally and Locally Optimized Detection (TALOD) method~~, and applied it to 10-minute interval ~~real-time~~SLH data observed ~~by the using a~~ MIROS ~~rRange-fFinder~~ (SM-140) from 2003 to 2022 at the I-ORS. The TALOD method comprises is divided can be classified into both manual and automatic processes. The manual check is performed prior to the automated procedures and flags specific sections based primarily on historical metadata to enhance the performance of subsequent automated QC steps. ~~Before~~The automatic process consists of. ~~The manual process includes a METADATA manual check that relies on the empirical knowledge of the data producer. The METADATA manual check flags sections to that could contaminate the long term characteristics of the collected time series observations. This check improves the performance of subsequent automatic QC processes. The automatic process includes RANGE, SPIK, and STUCK range, spike, and stuck checks. The range check utilized residual components, with residual components derived from the tidal prediction model, TPX09 tidal prediction model, allowing it to may enable it to address known issues such as detection failure due caused by to non-periodic outliers or adulteration contamination during when estimating the tidal components estimation using through the least squares method. Spatiotemporally optimized thresholds are applied in the spike check to reduce misclassifications and detection failures, particularly those caused by reduce misclassification and detection failures caused by frequent recurring erroneous r-values, during the spike check. By The spike check detects bad data by setting these a spatially and temporally optimized thresholds using non the non-tidal residuals components, the spike check outperforms traditional This approach can reduce false detections compared to the gradient-based GSM, which Also In addition, the GSM method tends to incorrectly flag detect rapidly fluctuating SLH, such as extreme weather events, as an~~

outliers. In the stuck check, we incorporated also utilized the reoccurrence frequency of specific values to handle the alternation between the good and bad data, which are the unique characteristics of SLH at the I-ORS. This study confirmed that the novel stuck check, which leverages the reoccurrence rate of the identical values same value over a defined time period, for a specific period can reduce truncation and increase the retention rate of good valid data compared to with existing QC processes.

~~such as IO the KHOA method. The newly identified error characteristics and corresponding detection methods presented in this study may serve as valuable components in both existing and future observational programs. It is also worth noting that integrating all or part of TALOD into established quality control process such as SELENE may holds promise for enhancing data quality and contributing to future observational activities in the open ocean. To evaluate the reliability of SLH data applying the TALOD and analyze the characteristics of SLH data from various institutions, we collected and compared with HYCOM, Satellite, GLORYS, and ORAS5. Before 2018, HYCOM Ra and Satellite data altimetry data exhibited the highest performance, while GLORYS and ORAS5 showed relatively higher RMSEs. Since 2018, the trend of SLH for HYCOM (HYCOM Sb) was 23.86 mm/yr, which showed unrealistic results compared to other datasets. In conclusion, the reanalysis data, including HYCOM Ra and satellite altimetry, showed a more similar pattern to the observation, and the others exhibited a quite narrower anomaly distribution for anomalies. Through assessment, we confirmed not only an issue with the variability of SLH in HYCOM, but also the reliability and validity of the TALOD QC method and SLH observation at the I-ORS.~~

The TALOD QC process includes the extreme event flag (EEF), which indicates the periods during which when SLH is affected by extreme weather events. For instance, since during the variance in of SLH was more than four times larger (including flagged data) than usual during the typhoon-influenced affected periods, the variance in SLH was frequently more than four times larger (including flagged data) than under normal conditions, increasing the likelihood that some good data may be mistakenly flagged some good data can could be flagged as range or and spike errors. Ensuring Because sufficient observational numbers data are essential for is crucial for research on typhoon-related processes, the EEF allows. Therefore, we provide an the extreme event option, enabling so researchers can use these to selectively include these utilize the data in their analysis to investigate the dynamics of for studies about extreme weather dynamics events.

In the SLR budget analysis, the BARYS effect related associated with the mass exchange between the ocean and land contributed significantly; was the primary contributor, accounting for approximately 70% of the total sea level change trend. The discrepancy in the difference in sea level trend between observations the from the I-ORS and

satellite altimetry (~~about approximately~~ 2.67 mm/yr) ~~can be was~~ attributed to VLM. The total VLM estimated from reanalysis data (-2.17 mm/yr) indicates ~~that~~ considerable ground subsidence ~~at of~~ the I-ORS site, ~~driven. In detail, this subsidence was more influenced~~ by local processes ~~rather~~ than ~~by~~ natural processes, ~~such as BS or GIA.~~ Although the ~~estimated total~~-VLM varies depending on the reanalysis data, the GNSS-measurebased observations of vertical displacement ~~trend~~ from 2013 to 2019 ~~also showed was a calculated trend of at~~ 0.89±0.47 mm/yr, ~~further confirming demonstrating~~ the ongoing ground subsidence at the I-ORS.

Despite the advancements ~~in the of~~ TALOD QC-process, several challenges remain. The ~~current implementation of the~~ TALOD QC process ~~is limited to delayed-mode only targets the observed~~ SLH data and is ~~still~~ not yet fully automated. ~~Additionally Moreover, additional there is a need for further~~ procedures are required to account for ~~sses that make it possible to take count of~~ misclassification ~~during in~~ extreme weather, such as rogue waves. In normal cases, good data with extreme values induced by the inverted barometer and steric effects may be erroneously identified as errors. Thus, ~~a an additional supplementary~~ -step ~~involving the adjustment of detection thresholds using simultaneously observed buddy variables—such as air/water temperatures, wind, and sea level pressure of adjusting coefficients using atmospheric and oceanographic observational variables~~—is required to improve accuracy.

Nevertheless, the TALOD QC process ~~has~~ is versatile enough to be applied to ~~the utility of being applied to~~ both tide gauges and range-finders. It also ~~enhances utilizes the predicted tidal components for each point, enhancing its adaptability by utilizing predicted tidal components for each location.~~ Well-controlled in-situ data are essential not only for data assimilation and validation but also for data management. The I-ORS platform stands out as a unique resource, offering ~~more than over 20 twenty~~ years of continuous ~~sea level obsatmospheric and oceanographic observations~~, along with various air-sea monitoring data in ~~data in the~~ central East China Sea ~~open sea.~~ Along with the I-ORS, ~~Additionally In addition,~~ two northern stations—the Gageocho Ocean Research Station (G-ORS) and Socheongcho Ocean Research Station (S-ORS)—can support studies on the propagation of oceanic and atmospheric signals ~~between are positioned along the meridian, contributing to the study studies of marine environmental development~~ marginal seas and the open ocean, ranging from extreme weather to climate variability.

## Acknowledgement

We ~~wish to thank~~ would like to thank the ~~the anonymous~~ reviewers for their detailed and ~~pertinent~~ constructive comments, which significantly ~~that helped to greatly~~ improved the quality of the manuscript ~~paper~~. This research

was supported by Korea Institute of Marine Science & Technology Promotion (KIMST) funded by the Ministry of Oceans and Fisheries (RS-2021-KS211502~~and RS 2022 KS221544~~); ~~and by the Korea Institute of Ocean Science & Technology (PEA0201).~~

#### **Data availability**

The SLH time series observed at the I-ORS are available from the KIOST repository (<https://doi.or.kr/10.22808/DATA-2024-8>).

#### **Supplement**

#### **Author contributions**

T-BJ developed the TALOD QC procedure and wrote the first draft with plotting figures. Taek-bum Jeong: ~~Development of TALOD QC and writing of first draft~~ Conceptualization, Methodology, Formal analysis, Writing—original draft, Writing—review & editing; YSK proposed the TALOD QC and this manuscript; and the concept for contributed to writing and revising the this manuscript, and contributed to both writing and revising the manuscript; Yong-Sun Kim: Conceptualization, Methodology, Validation, Writing—review & editing, second contact author ~~Proposal of TALOD QC and this manuscript, writing and revising this manuscript~~; HSC conducted the budget analysis of the sea level trend; Hyeosoo Cha: ~~Budget analysis in sea level trend; Conceptualization, Methodology, Validation, Writing—review & editing~~; Kwang-Young Jeong: ~~processed the data with~~ using KHOA QC method; Conceptualization, Methodology, Writing—review & editing; Mi Jin Jang: Conceptualization, Methodology, Writing—review & editing; J-YJ provided the I-ORS SLH data and processed the GNSS observations to calculated the vertical displacement; Jin-Yong Jeong: Conceptualization, Methodology, Writing—review & editing; ~~Data achievement and providing, GNSS processing~~; J-HL conducted ~~conducted~~ an overall analysis of the research results and contributed to improving the quality of the manuscript; Jae-Ho Lee: ~~Managing and writing as a corresponding author~~ Conceptualization, Methodology, Validation, Writing—review & editing, first contact author.

#### **Competing interests**

The contact author has declared that none of the authors has any competing interests.

## Special issue statement

This article is part of the special issue “Oceanography at coastal scales: modelling, coupling, observations, and applications”.

## Acknowledgements

This research was supported by Korea Institute of Marine Science & Technology Promotion (KIMST) funded by the Ministry of Oceans and Fisheries (RS-2021-KS211502 and RS-2022-KS221544), and by the Korea Institute of Ocean Science & Technology (PEA0201).

## References

- Calafat, F. M., Wahl, T., Tadesse, M. G., and Sparrow, S. N.: Trends in Europe storm surge extremes match the rate of sea-level rise, *Nature*, 603, 841–845. <https://doi.org/10.1038/s41586-022-04426-5>, 2022.
- Calafat, F. M., Wahl, T., Tadesse, M. G., and Sparrow, S. N.: Trends in Europe storm surge extremes match the rate of sea-level rise, *Nature*, 603, 841–845. <https://doi.org/10.1038/s41586-022-04426-5>, 2022.
- Caron, L., Ivins, E. R., Larour, E., Adhikari, S., Nilsson, J., and Blewitt, G.: GIA model statistics for GRACE hydrology, cryosphere, and ocean science, *Geophys. Res. Lett.*, 45, 2203–2212. <https://doi.org/10.1002/2017GL076644>, 2018.
- Cayan, D. R., Bromirski, P. D., Hayhoe, K., Tyree, M., Dettinger, M. D., and Flick, R. E.: Climate change projections of sea level extremes along the California coast, *Climatic Change*, 87, 57–73, 2008. a.
- Cazenave, A., Meyssignac, B., Ablain, M., Balmaseda, M., Bamber, J., Barletta, V., Beckley, B., Benveniste, J., Berthier, E., and Blazquez, A.: Global sea-level budget 1993-present, 2018. a.
- Cha, H., Jo, S., and Moon, J.-H.: A process-based relative sea-level budget along the coast of Korean peninsula over 1993–2018, *Ocean Polar Res.*, 46, 31–42, 2024. a, b, c.
- Cha, H., Moon, J.-H., Kim, T., and Song, Y. T.: A process-based assessment of the sea-level rise in the northwestern Pacific marginal seas, *Communications, Earth Environ.*, 4, 300, 2023. a, b.
- Chen, X., Zhang, X., Church, J. A., Watson, C. S., King, M. A., Monselesan, D., Legresy, B., and Harig, C.: The increasing rate of global mean sea-level rise during 1993–2014, *Nat. Clim. Change*, 7, 492–495. <https://doi.org/10.1038/nclimate3325>, 2017.



- Cheng, L., Trenberth, K. E., Fasullo, J., Boyer, T., Abraham, J., and Zhu, J.: Improved estimates of ocean heat content from 1960 to 2015, *Sci. Adv.*, 3, e1601545. <https://doi.org/10.1126/sciadv.1601545>, 2017.
- Dieng, H. B., Cazenave, A., Meyssignac, B., and Ablain, M.: New estimate of the current rate of sea level rise from a sea level budget approach, *Geophys. Res. Lett.*, 44, 3744–3751. <https://doi.org/10.1002/2017GL073308>, 2017.
- Erofeeva, S. and Egbert, G. D.: TPXO9—a new global tidal model in TPXO series Ocean Sciences Meeting, 2018. a, 2018.
- ~~Fox-Kemper, B., Hewitt, H. T., Xiao, C., Aðalgeirsdóttir, G., Drijfhout, S. S., Edwards, T. L., Golledge, N. R., Hemer, M., Kopp, R. E., Krinner, G., Mix, A., Notz, D., Nowicki, S., Nurhati, I. S., Ruiz, L., Sallée, J.-B., Slangen, A. B. A., and Yu, Y.: Ocean, Cryosphere and Sea Level Change, in: Climate Change 2021: The Physical Science Basis. Contribution of Working Group I to the Sixth Assessment Report of the Intergovernmental Panel on Climate Change, edited by Masson-Delmotte, V., Zhai, P., Pirani, A., Connors, S., Péan, C., Berger, S., Caud, N., Chen, Y., Goldfarb, L., Gomis, M., Huang, M., Leitzell, K., Lonnoy, E., Matthews, J., Maycock, T., Waterfield, T., Yelekçi, O., Yu, R., and Zhou, B., p. 1211–1362, Cambridge University Press, Cambridge, United Kingdom and New York, NY, USA, <https://doi.org/doi:10.1017/9781009157896.011>, 2021. a, b.~~  
~~Fox-Kemper, B., Hewitt, H., Xiao, C., Aðalgeirsdóttir, G., Drijfhout, S., Edwards, T., Golledge, N., Hemer, M., Kopp, R., and Krinner, G.: Ocean, cryosphere and sea level change: Climate change, 2021. a, edited by Zhai, P., A. Pirani, editor, 2021: the physical science basis. Contribution of Working Group I to the Sixth Assessment Report of the Intergovernmental Panel on Climate Change.~~
- Frederikse, T., Landerer, F., Caron, L., Adhikari, S., Parkes, D., Humphrey, V. W., Dangendorf, S., Hogarth, P., Zanna, L., Cheng, L.: The causes of sea-level rise since 1900, *Nature*, 584, 393–397. <https://doi.org/10.1038/s41586-020-2591-3>, 2020. a, b.
- Good, S. A., Martin, M. J., and Rayner, N. A.: EN4: Quality controlled ocean temperature and salinity profiles and monthly objective analyses with uncertainty estimates, *JGR Oceans*, 118, 6704–6716. <https://doi.org/10.1002/2013JC009067>, 2013.
- Gregory, J. M., Griffies, S. M., Hughes, C. W., Lowe, J. A., Church, J. A., Fukimori, I., Gomez, N., Kopp, R. E., Landerer, F., and Cozannet, G. L.: Concepts and terminology for sea level: Mean, variability and change, both local and global, *Surveys in Geophysics*, 40, 1251–1289, 2019. a, b, c.



- Ha, K.-J., Nam, S., Jeong, J.-Y., Moon, I.-J., Lee, M., Yun, J., Jang, C. J., Kim, Y. S., Byun, D.-S., Heo, K.-Y., Shim, J.-S.: Observations utilizing Korea ocean research stations and their applications for process studies, *Bull. Am. Meteorol. Soc.*, 100, 2061–2075. <https://doi.org/10.1175/BAMS-D-18-0305.1>, 2019.
- Hamlington, B. D., Gardner, A. S., Ivins, E., Lenaerts, J. T., Reager, J., Trossman, D. S., Zaron, E. D., Adhikari, S., Arendt, A., and Aschwanden, A.: Understanding of contemporary regional sea-level change and the implications for the future, *Reviews of Geophysics*, 58, RG000672, e2019, 2020. a.
- Han, G., Ma, Z., Bao, H., and Slangen, A.: Regional differences of relative sea level changes in the northwest Atlantic: Historical trends and future projections, *JGR Oceans*, 119, 156–164. <https://doi.org/10.1002/2013JC009454>, 2014.
- Hwang, Y., Do, K., Jeong, J. Y., Lee, E., and Shin, S.: Algorithm development for quality control of rangefinder wave time series data at ocean research station, *J. Coast. Disaster Prev.*, 9, 171–178. <https://doi.org/10.20481/kscdp.2022.9.3.171>, 2022.
- IOC: GTSP Real-Time Quality Control Manual, Intergovernmental Oceanographic Commission, 1990.
- IOC: Manual of Quality Control Procedures for Validation of Oceanographic Data, Intergovernmental Oceanographic Commission, 1993.
- Ishii, M., Fukuda, Y., Hirahara, S., Yasui, S., Suzuki, T., and Sato, K.: Accuracy of global upper ocean heat content estimation expected from present observational data sets, *Sola*, 13, 163–167, 2017. a.
- Jean-Michel, L., Eric, G., Romain, B.-B., Gilles, G., Angélique, M., Marie, D., Clément, B., Mathieu, H., Olivier, L. G., and Charly, R.: The Copernicus global 1/12 oceanic and sea ice GLORYS12 reanalysis, *Front. Earth Sci.*, 9, 698876, 2021. a.
- KHOA (Korea Hydrographic and Oceanographic Agency): Analysis and prediction of sea level change, 2013.
- Kim, D.-Y., Park, S.-H., Woo, S.-B., Jeong, K.-Y., and Lee, E.-I.: Sea level rise and storm surge around the southeastern coast of Korea, *J. Coast. Res.*, 79, 239–243. <https://doi.org/10.2112/SI79-049.1>, 2017. a.
- Kim, G.-U., Lee, J., Kim, Y. S., Noh, J. H., Kwon, Y. S., Lee, H., Lee, M., Jeong, J., Hyun, M. J., Won, J., Jeong, J.-Y.: Impact of vertical stratification on the 2020 spring bloom in the Yellow Sea, *Sci. Rep.*, 13, 14320. <https://doi.org/10.1038/s41598-023-40503-z>, 2023b.
- Kim, G.-U., Lee, K., Lee, J., Jeong, J.-Y., Lee, M., Jang, C. J., Ha, K.-J., Nam, S., Noh, J. H., and Kim, Y. S.: Record-breaking slow temperature evolution of spring water during 2020 and its impacts on spring bloom in the Yellow Sea, *Front. Mar. Sci.*, 9, 824361. <https://doi.org/10.3389/fmars.2022.824361>, 2022.

- Kim, G.-U., Oh, H., Kim, Y. S., Son, J.-H., and Jeong, J.-Y.: Causes for an extreme cold condition over NorthEast Asia during April 2020, *Sci. Rep.*, 13, 3315. <https://doi.org/10.1038/s41598-023-29934-w>, 2023<sup>a, a, b</sup>.
- Kim, K.-Y. and Kim, Y.: A comparison of sea level projections based on the observed and reconstructed sea level data around the Korean Peninsula, *Climatic Change*, 142, 23–36, 2017. a.
- Kim, Y. S., Jang, C. J., Noh, J. H., Kim, K.-T., Kwon, J.-I., Min, Y., Jeong, J., Lee, J., Min, I.-K., Shim, J.-S., Byun, D.-S., Kim, J., Jeong, J.-Y.: A Yellow Sea monitoring platform and its scientific applications, *Front. Mar. Sci.*, 6, 601. <https://doi.org/10.3389/fmars.2019.00601>, 2019. \_
- Kulp, S. A. and Strauss, B. H.: New elevation data triple estimates of global vulnerability to sea-level rise and coastal flooding, *Nature Communications*, 10, 1–12, 2019. a.
- Lee, J. H., Lozovatsky, I., Jang, S. T., Jang, C. J., Hong, C. S., and Fernando, H. J. S.: Episodes of nonlinear internal waves in the northern East China Sea, *Geophys. Res. Lett.*, 33. <https://doi.org/10.1029/2006GL027136>, 2006. a, b.
- Lee, K., Nam, S., Cho, Y.-K., Jeong, K.-Y., and Byun, D.-S.: Determination of long-term (1993–2019) sea level rise trends around the Korean peninsula using ocean tide-corrected, multi-mission satellite altimetry data, *Front. Mar. Sci.*, 9, 810549. <https://doi.org/10.3389/fmars.2022.810549>, 2022. a, b, c.
- Li, Y., Feng, J., Yang, X., Zhang, S., Chao, G., Zhao, L., and Fu, H.: Analysis of sea level variability and its contributions in the Bohai, Yellow Sea, and East China Sea, *Front. Mar. Sci.*, 11, 1381187. <https://doi.org/10.3389/fmars.2024.1381187>, 2024.
- [Lin-Ye, J., Pérez Gómez, B., Gallardo, A., Manzano, F., de Alfonso, M., Bradshaw, E., and Hibbert, A.: Delayed-mode reprocessing of in situ sea level data for the Copernicus Marine Service, \*Ocean Sci.\*, 19, 1743–1751, <https://doi.org/10.5194/os-19-1743-2023>, 2023.](#)
- Ludwigsen, C. B., Andersen, O. B., Marzeion, B., Malles, J.-H., Müller Schmied, H., Döll, P., Watson, C., and King, M. A.: Global and regional ocean mass budget closure since 2003, *Nat. Commun.*, 15, 1416. <https://doi.org/10.1038/s41467-024-45726-w>, 2024.
- Min, Y., Jeong, J.-Y., Jang, C. J., Lee, J., Jeong, J., Min, I.-K., Shim, J.-S., and Kim, Y. S.: Quality control of observed temperature time series from the Korea ocean research stations: Preliminary application of ocean observation initiative’s approach and its limitation, *Ocean Polar Res.*, 42, 195–210, 2020. a, b, e.
- Min, Y., Jun, H., Jeong, J.-Y., Park, S.-H., Lee, J., Jeong, J., Min, I., and Kim, Y. S.: Evaluation of international quality control procedures for detecting outliers in water temperature time-series at Jeodo ocean research station, *Ocean Polar Res.*, 43, 229–243, 2021. a.

Moon, I.-J., Shim, J.-S., Lee, D. Y., Lee, J. H., Min, I.-K., and Lim, K. C.: Typhoon researches using the Jeodo Ocean Research Station: Part I. Importance and present status of typhoon observation, *Atmosphere*, 20, 247–260, 2010. a.

Nerem, R. S., Beckley, B. D., Fasullo, J. T., Hamlington, B. D., Masters, D., and Mitchum, G. T.: Climate-change–driven accelerated sea-level rise detected in the altimeter era, *Proc. Natl Acad. Sci. U. S. A.*, 115, 2022–2025. <https://doi.org/10.1073/pnas.1717312115>, 2018.

NOAA: NDBC Handbook of Automated Data Quality Control Checks and Procedures, National Data Buoy Center, National Oceanic and Atmospheric Administration, 2009.

OOI, Protocols and procedures for OOI data products: QA, QC, calibration, physical samples, version 1-22. Consortium for Ocean Leadership, [https://oceanobservatories.org/wp-content/uploads/2015/09/1102-00300\\_Protocols\\_Procedures\\_Data\\_Products\\_QAQC\\_Cal\\_Physical\\_Samples\\_OOI](https://oceanobservatories.org/wp-content/uploads/2015/09/1102-00300_Protocols_Procedures_Data_Products_QAQC_Cal_Physical_Samples_OOI), Last accessed: 30 September 2019, 2013. a-

Park, J. H., Yeo, D. E., Lee, K., Lee, H., Lee, S. W., Noh, S., Kim, S., Shin, J., Choi, Y., and Nam, S.: Rapid decay of slowly moving Typhoon Soulik (2018) due to interactions with the strongly stratified northern East China Sea, *Geophys. Res. Lett.*, 46, 14595–14603, 2019. a.

Pawlowicz, R., Beardsley, B., and Lentz, S.: Classical tidal harmonic analysis including error estimates in MATLAB using T\_TIDE, *Comput. Geosci.*, 28, 929–937. [https://doi.org/10.1016/S0098-3004\(02\)00013-4](https://doi.org/10.1016/S0098-3004(02)00013-4), 2002.

Pirooznia, M., Rouhollah Emadi, S., and Najafi Alamdari, M.: Caspian Sea tidal modelling using coastal tide gauge data, *J. Geol. Res.*, 2016, 1–10. <https://doi.org/10.1155/2016/6416917>, 2016.

Pirooznia, M., Raoofian Naeeni, M., and Amerian, Y.: A Comparative Study Between Least Square and Total Least Square Methods for Time–Series Analysis and Quality Control of Sea Level Observations, *Marine Geodesy*, 42(2), 104–129, <https://doi.org/10.1080/01490419.2018.1553806>, 2019.

~~Pörtner, H. O., Roberts, D. C., Masson Delmotte, V., Zhai, P., Tignor, M., Poloczanska, E., and Weyer, N.: The ocean and cryosphere in a changing climate, IPCC special report on the ocean and cryosphere in a changing climate, 1155, 10.1017, 2019. a-~~

Pugh, D.: Tides, surges and mean sea-level, 555, John Wiley & Sons, Bath Typesetting Limited, Great Britain, 1987. a.

- Pugh, D. T., Abualnaja, Y., and Jarosz, E.: The tides of the Red Sea, in: *Oceanographic and Biological Aspects of the Red Sea*, edited by Rasul, N. M. A. and Stewart, I. C. F., pp. 11–40, Springer, Cham, 2019.
- Pytharoulis, S., Chaikalis, S., and Stiros, S. C.: Uncertainty and bias in electronic tide-gauge records: Evidence from collocated sensors, *Measurement*, 125, 496–508, 2018. a.
- Roemmich, D., Gilson, J., Davis, R., Sutton, P., Wijffels, S., and Riser, S.: Decadal spinup of the South Pacific subtropical gyre, *J. Phys. Oceanogr.*, 37, 162–173. <https://doi.org/10.1175/JPO3004.1>, 2007.
- Royston, S., Dutt Vishwakarma, B., Westaway, R., Rougier, J., Sha, Z., and Bamber, J.: Can we resolve the basin-scale sea level trend budget from GRACE ocean mass?, *JGR Oceans*, 125, JC015535, e2019. <https://doi.org/10.1029/2019JC015535>, 2020.
- Saranya, J. S., Dasgupta, P., and Nam, S.: Interaction between typhoon, marine heatwaves, and internal tides: Observational insights from Jeju Ocean Research Station in the northern East China Sea, *Geophys. Res. Lett.*, 51, GL109497, e2024. <https://doi.org/10.1029/2024GL109497>, 2024.
- Yang, S., Moon, I.-J., Bae, H.-J., Kim, B.-M., Byun, D.-S., and Lee, H.-Y.: Intense atmospheric frontogenesis by air–sea coupling processes during the passage of Typhoon Lingling captured at Jeju Ocean Research Station, *Scientific Reports*, *Sci. Rep.*, 12, 15513. <https://doi.org/10.1038/s41598-022-19359-2>, 2022.
- Yin, J., Griffies, S. M., Winton, M., Zhao, M., and Zanna, L.: Response of storm-related extreme sea level along the US Atlantic coast to combined weather and climate forcing, *J. Clim.*, 33, 3745–3769. <https://doi.org/10.1175/JCLI-D-19-0551.1>, 2020.
- Zuo, H., Balmaseda, M. A., Tietsche, S., Mogensen, K., and Mayer, M.: The ECMWF operational ensemble reanalysis–analysis system for ocean and sea ice: A description of the system and assessment, *Ocean science*, 15, 779–808, 2019. a.

891    **List of Table**

892    Table 1. Instrument specifications for the MIROS SM-140.

893    Table 2. List of Typhoon cases during observation.

894    Table 3. Detection counts and proportions for each flag from Oct 2003 to Dec 2022 (excluding NaN values).

895    Table 4: Differences in flag detection methods between TALOD and KHOA.

896

## List of Figures

Figure 1. The structure of I-ORS and Instruments (Right) and the horizontal distribution for bathymetry and the tracks of typhoons passed by I-ORS (data from Joint Typhoon Warning Center; cases depicted in Fig. 6).

[The star marks indicate the location of the I-ORS \(red\) and the Socheongcho \(black, north\) and Gageocho \(black, south\) Ocean Research Stations. The star marks indicate the location of the I-ORS \(red\) and the Socheongcho \(black; above\) and Gageocho \(black; below\) Ocean Research Station, respectively.](#) The black dots depict the locations of tide stations. The grey solid lines show the storm tracks passing by I-ORS from 2003 to 2022 (Table 2). The darker lines indicate the typhoon case in Fig. 6.

Figure 2. The circle markers indicate each process of methodological adjustment for the data before TP. The grey line with circles means the raw data and the lines with blue triangle and red square indicate the reverse and shift (+ 1.57m after reversed) process.

Figure 3. Flow chart of TALOD QC process.

Figure 4. Lines indicate the processes for fitting TPXO9 to [the](#) observation (black line with circle) in the range check. (1) The blue line with a triangle means raw TPXO9 data. (2) The orange line with the square shows mean-shifted TPXO9 based on the Mean Square Error method. (3) The green line with a circle indicates the final output with a ~~twice-smoothed~~[twice-smoothed](#) bias added.

Figure 5. Time series for the examples of 4 flags. a) manual, b) stuck, c) range, and d) spike. Each marker indicates [gGood dData](#) (grey circle), manual (blue circle), range (green triangle), spike (yellow square with red outline), and stuck (red cross), respectively. [Time series of the non-tidal residual component corresponding to Fig. 5 is provided in the Supplement \(Fig. S1\).](#)

Figure 6. Time series of sea level anomalies for typhoon cases. a) Bolaven in 2012, b) Soulik in 2018, c) Lingling in 2019, and d) Bavi in 2020. Good [dData](#) (grey circle), EEF (purple circle), range (green triangle), and spike (yellow square with red outline), respectively. [Time series of the non-tidal residual component corresponding to Fig. 6 is provided in the Supplement \(Fig. S2\).](#)

Figure 7. Representative results from 01 Apr 2012 to 15 Apr 2012.

Figure 8. Same as Fig. 5, but for invariant stuck case (a-b, from 05 May 2005 to 07 May 2005), stuck case during short-period (c-d, from 12 Jul 2013 to 18 Jul 2013), and range-spike misclassification case (e-f, from 12 Jun 2016 to 14 Jun 2016). The figures on the left and right sides show results for TALOD and KHOA, respectively. For illustrative purposes, only the flags generated by the automatic QC process were considered in panel f. [Comparison results with SELENE are provided in the Supplement \(Fig. S3\).](#)

Figure 9. Histogram of observed sea level anomalies without QC (light red), with QC (light grey), QCed by KHOA method (dark grey) from 2003 to 2022 at the I-ORS. The area enclosed by a darker grey line indicates the normal distribution.

Figure 10. Time series of [daily mean sea level data after QC](#) ~~daily QC-ed observations~~ (black dot), [Satellite altimetry](#) (green empty circle), HYCOM (light red diamond), and GLORYS12 (light cyan hexagram) data during the observation period at the I-ORS.

Figure 11. Bar plot with error bar (A; Left) and modified Taylor diagram (B; Right). The azimuthal angle represents the correlation coefficient, the radial distance indicates the standard deviation, and the semicircles centered at the “OBS” marker mean the Root Mean Square Errors. The colors and markers indicate each dataset (black circle: observation, green square: satellite altimetry, purple pentagram: ORAS5, light cyan hexagram: GLORYS, red diamond: HYCOM, light red upward-pointing triangle: HYCOM-R, dark red downward-pointing triangle: HYCOM-S).

Figure 12. Monthly time series of sea level anomalies (left) and sea level rise rates (right; units: mm/yr). Each color and type of line indicates the dataset (OBS: black solid line, Satellite: green dotted line, Sum: bright red circle, STERO: orange diamond, BARY: purple dotted line, GIA: sea green dashed line, and GNSS: dark brown).

---

Table 1. Instrument specifications for the MIROS SM 140.

<u>Data</u>	<u>Range</u>	<u>Resolution</u>	<u>Accuracy</u>
<u>Range</u>	<u>1–23 m</u> <u>2–95 m</u>	<u>1 mm</u>	<u>±5 mm</u>
<u>Frequency</u>	<u>50–200 Hz (according to range)</u>		

Table 2. List of Typhoon during observation.

<u>Typhoon</u>	<u>Start date</u>	<u>End date</u>
<u>Chanthu (2021)</u>	<u>14 Sep. 2021</u>	<u>16 Sep. 2021</u>
<u>Bavi (2020)</u>	<u>25 Aug. 2020</u>	<u>26 Aug. 2020</u>
<u>Lingling (2019)</u>	<u>6 Sep. 2019</u>	<u>7 Sep. 2019</u>
<u>Kong-ree (2018)</u>	<u>6 Sep. 2018</u>	<u>7 Sep. 2018</u>
<u>Soulík (2018)</u>	<u>22 Aug. 2018</u>	<u>23 Aug. 2018</u>
<u>Chan-hom (2015)</u>	<u>12 Jul. 2015</u>	<u>12 Jul. 2015</u>
<u>Neoguri (2014)</u>	<u>9 Aug. 2014</u>	<u>9 Aug. 2014</u>
<u>Bolaven (2012)</u>	<u>27 Aug. 2012</u>	<u>28 Aug. 2012</u>
<u>Muifa (2011)</u>	<u>8 Aug. 2011</u>	<u>9 Aug. 2011</u>
<u>Megi (2004)</u>	<u>10 Aug. 2004</u>	<u>10 Aug. 2004</u>

Table 3. Detection counts and proportions for each flag from Oct 2003 to Dec 2022 (excluding NaN values).

<u>Flag number</u>	<u>1</u>	<u>2</u>	<u>4</u>	<u>5</u>	<u>7</u>	<u>8</u>
<u>(Name)</u>	<u>(Good data)</u>	<u>(Range)</u>	<u>(Spike)</u>	<u>(Stuck)</u>	<u>(Manual)</u>	<u>(NaN)</u>
<u>#</u>	<u>793,034</u>	<u>1,725</u>	<u>2,052</u>	<u>33,383</u>	<u>56,024</u>	<u>165,702</u>
<u>% (without NaN)</u>	<u>89.49%</u>	<u>0.19%</u>	<u>0.23%</u>	<u>3.77%</u>	<u>6.32%</u>	

Table 4: Differences in flag detection methods between TALOD and KHOA.

<u>Flag</u>	<u>TALOD</u>	<u>KHOA</u>
<u>Range</u>	<u>Data point where observation exceeds the threshold from the tidal component, which is adjusted according to temporal observations</u>	<u>Data point exceeds sensor or operator selected min/max for whole period</u>

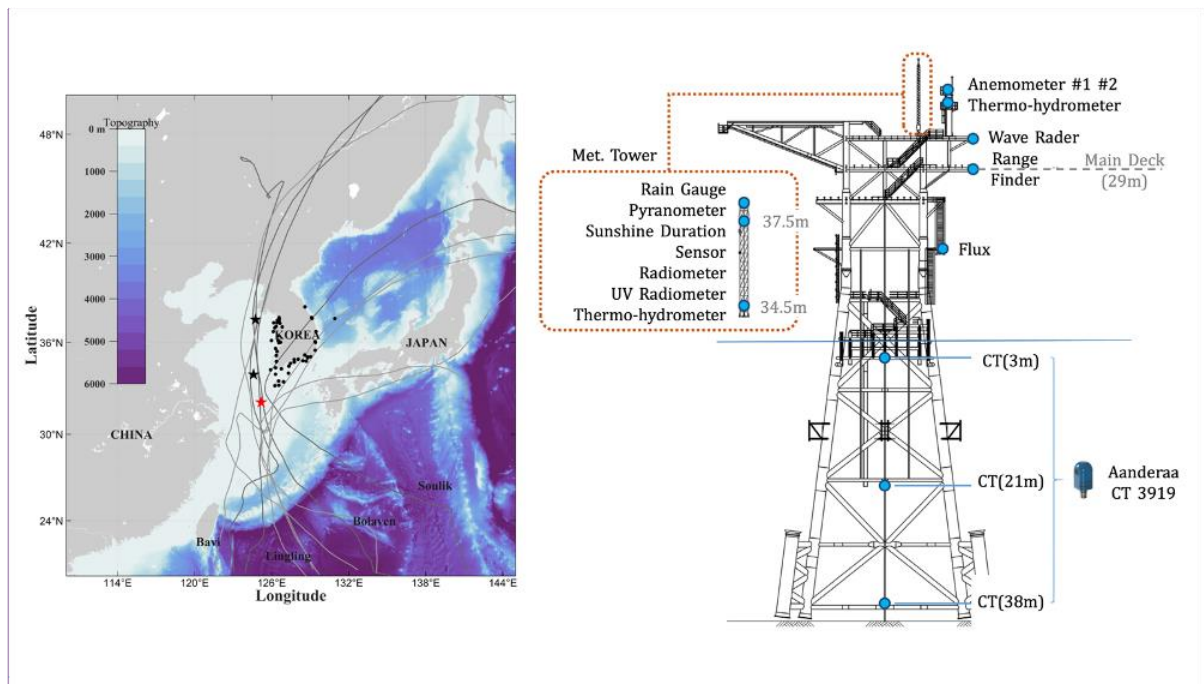


<u><b>SPIKE</b></u>	<u>Data point where the square of the difference in residuals exceeds the threshold</u>	<u>Data point <math>n-1</math> exceeds a selected threshold relative to adjacent data points</u>
<u><b>STUCK</b></u>	<u>Data point where the recurrence rates for constant value within the windows are over thresholds</u>	<u>Invariant value</u>

951

952

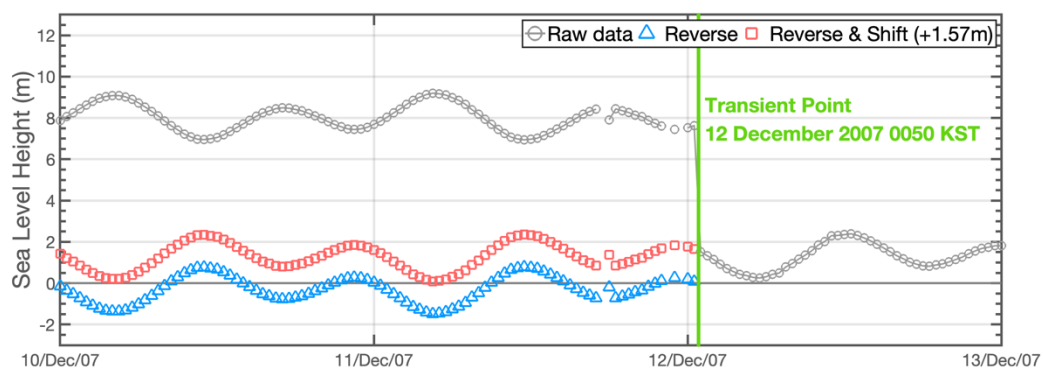
---



954

955 [\[TJ12\]](#)

956 [Figure 1. The structure of I-ORS and Instruments \(Right\) and the horizontal distribution for bathymetry and the](#)  
 957 [tracks of typhoons passed by I-ORS \(data from Joint Typhoon Warning Center \[YSK13\]; cases depicted in Fig. 6\).](#)  
 958 [The star marks indicate the location of the I-ORS \(red\) and the Socheongcho \(black; above\) and Gageocho \(black;](#)  
 959 [below\) Ocean Research Station, respectively. The black dots depict the locations of tide stations. The grey solid](#)  
 960 [lines show the storm tracks passing by I-ORS from 2003 to 2022 \(Table 2\). The darker lines indicate the typhoon](#)  
 961 [case in Fig. 6.](#)



962

963 [Figure 2. The circle markers indicate each process of methodological adjustment for the data before TP. The grey](#)  
 964 [line with circles means the raw data and the lines with blue triangle and red square indicate the reverse and shift](#)  
 965 [\(+ 1.57 m after reversed\) process.](#)

966

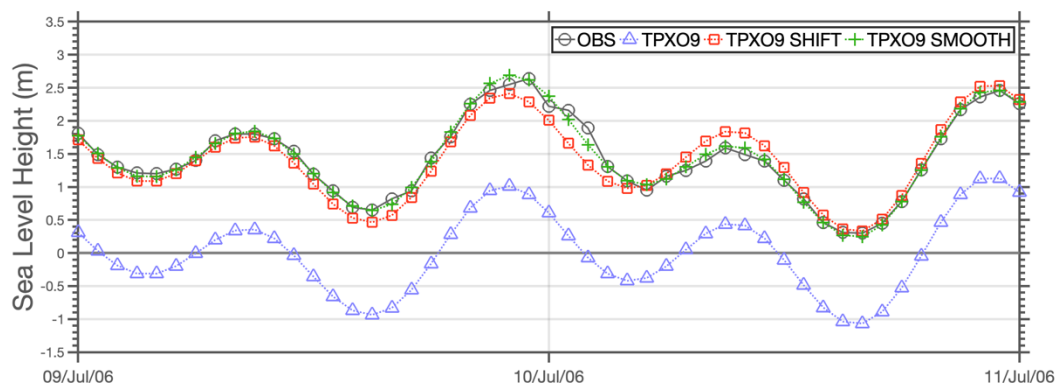


Figure 4. Lines indicate the processes for fitting TPXO9 to observation (black line with circle) in the range check. (1) The blue line with a triangle means raw TPXO9 data. (2) The orange line with the square shows mean shifted TPXO9 based on the mean square error method. (3) The green line with a circle indicates the final output with a twice-smoothed bias added.

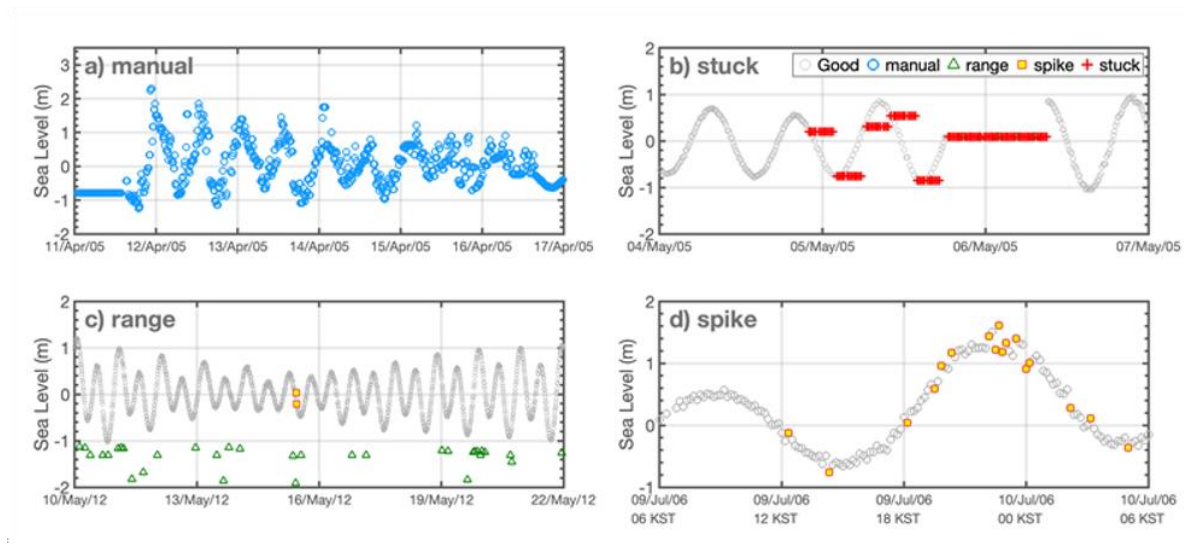


Figure 5. Time series for the examples of 4 flags. a) manual, b) stuck, c) range, and d) spike. Each marker indicates Good Data (grey circle), manual (blue circle), range (green triangle), spike (yellow square with red outline), and stuck (red cross), respectively.

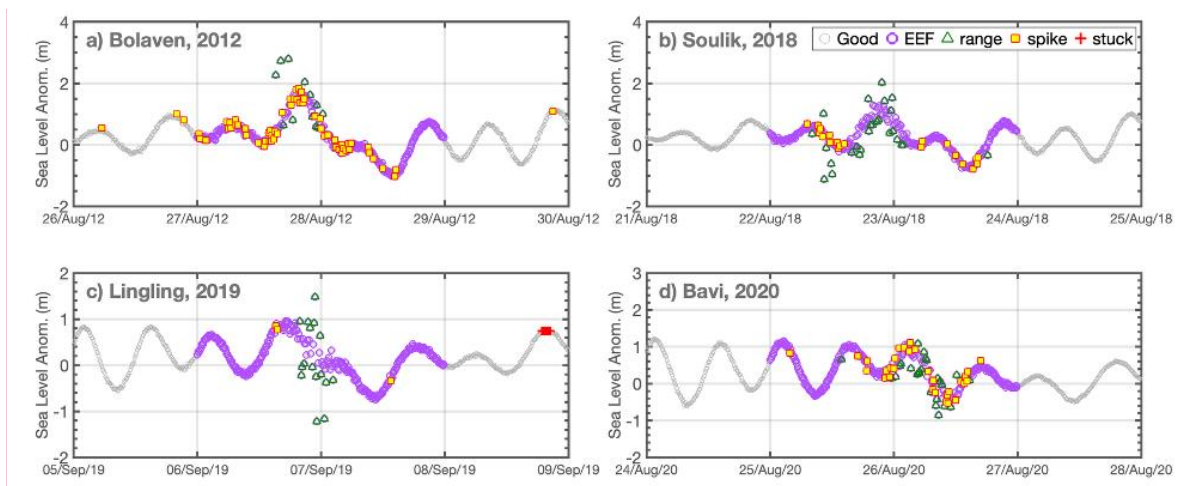


Figure 6. Time series of sea level anomalies for typhoon cases. a) Bolaven in 2012, b) Soulik in 2018, c) Lingling in 2019, and d) Bavi in 2020. Good Data (grey circle), EEf (purple circle), range (green triangle), and spike (yellow square with red outline), respectively.

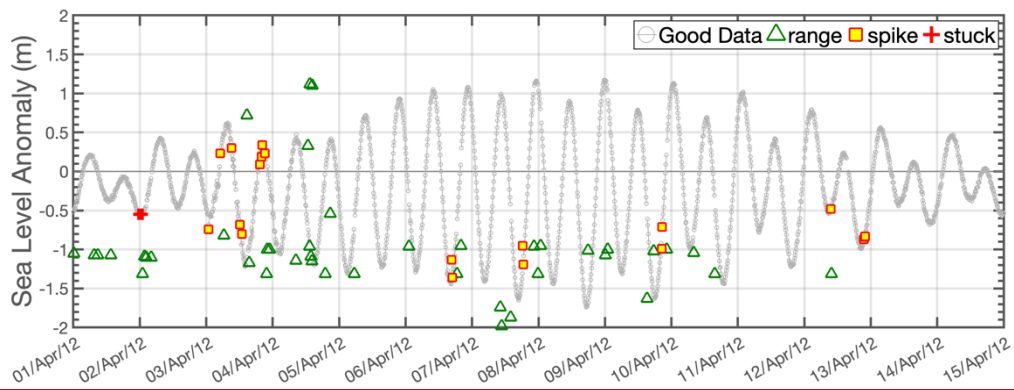


Figure 7. Representative results from 01 Apr 2012 to 15 Apr 2012.

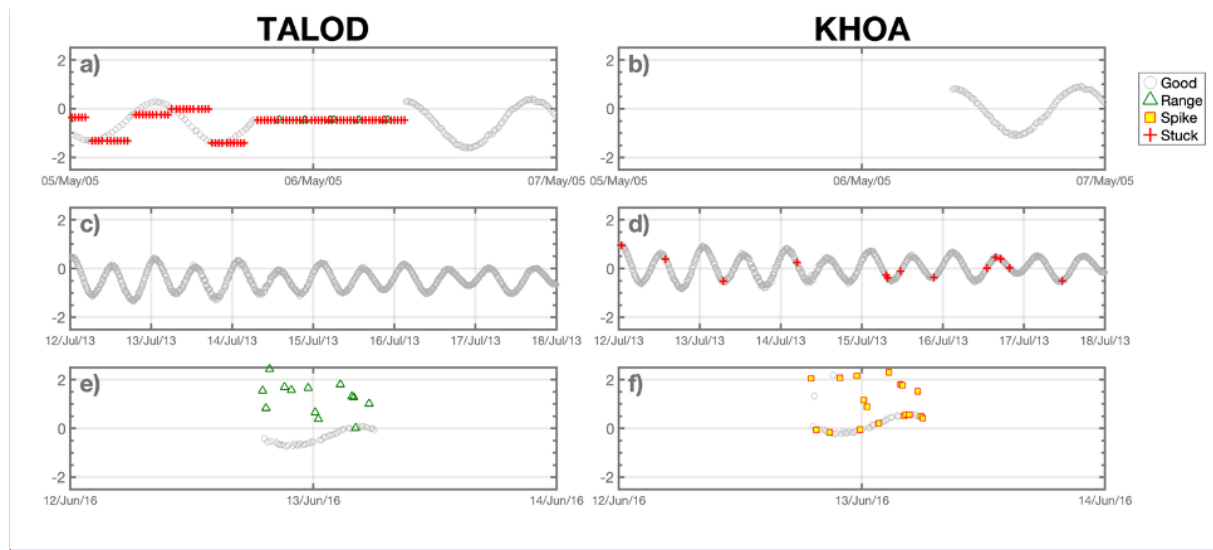


Figure 8. Same as Fig. 5, but for invariant stuck case (a-b, from 05 May 2005 to 07 May 2005), stuck case during short period (c-d, from 12 Jul 2013 to 18 Jul 2013), and range spike misclassification case (e-f, from 12 Jun 2016 to 14 Jun 2016). The figures on the left and right sides show results for TALOD and KHOA, respectively. For illustrative purposes, only the flags generated by the automatic QC process were considered in panel f.

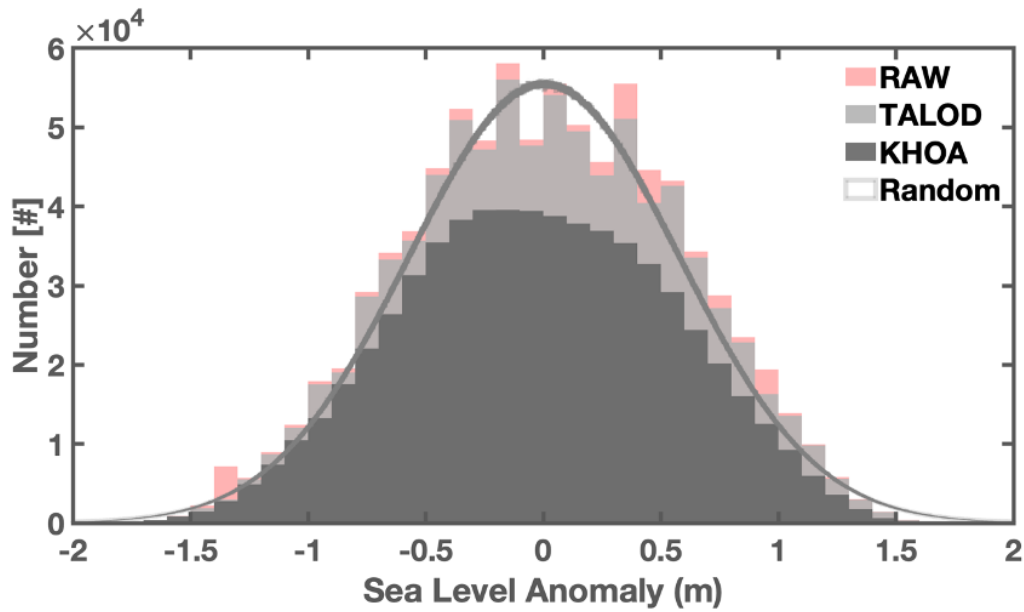


Figure 9. Histogram of observed sea level anomalies without QC (light red), with QC (light grey), QCed by KHOA method (dark grey) from 2003 to 2022 at the I ORS. The area enclosed by a darker grey line indicates the normal distribution.

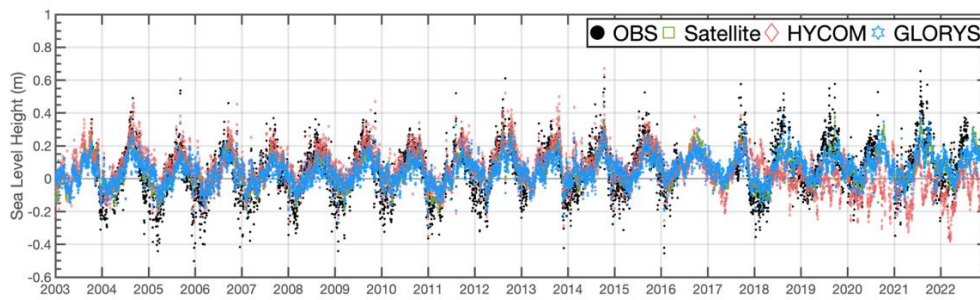


Figure 10. Time series of daily QC ed observations (black dot), Satellite (green empty circle), HYCOM (light red diamond), and GLORYS12 (light cyan hexagram) data during the observation period at the I ORS.

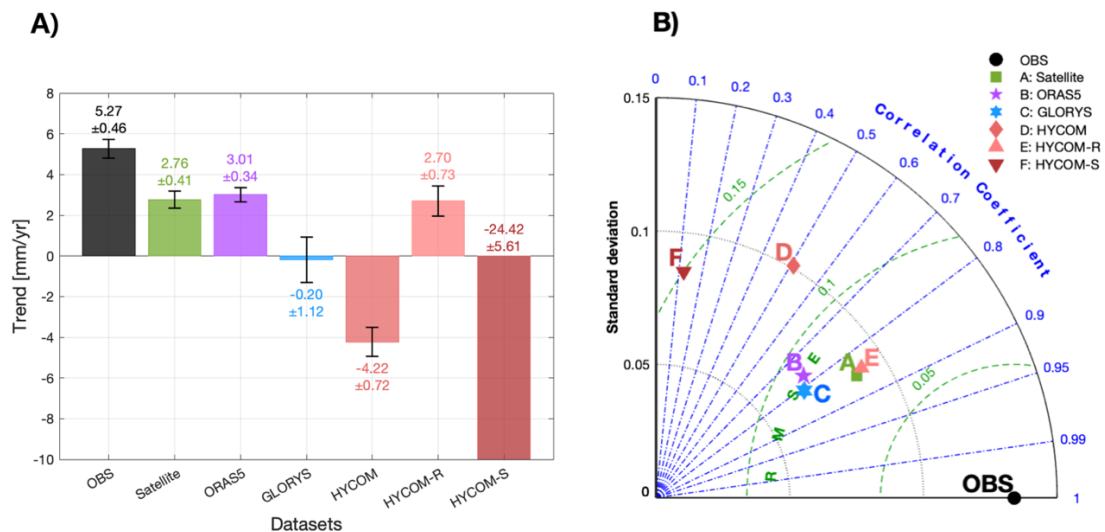


Figure 11. Bar plot with error bar (A; Left) and modified Taylor diagram (B; Right). The azimuthal angle represents the correlation coefficient, the radial distance indicates the standard deviation, and the semicircles centered at the “OBS” marker mean the Root Mean Square Errors. The colors and markers indicate each dataset (black circle: observation, green square: satellite altimetry, purple pentagram: OPAS5, light cyan hexagram: GLORYS, red diamond: HYCOM, light red upward pointing triangle: HYCOM R, dark red downward pointing triangle: HYCOM S).



Figure 12. Monthly time series of sea level anomalies (left) and sea level rise rates (right; units: mm/yr). Each color and type of line indicates the dataset (OBS: black solid line, Satellite: green dotted line, Sum: bright red circle, STERO: orange diamond, BARY: purple dotted line, GIA: sea green dashed line, and GNSS: dark brown).